Trends in Analytical Chemistry 191 (2025) 118353

Contents lists available at ScienceDirect

Trends in Analytical Chemistry

journal homepage: www.elsevier.com/locate/trac

Surface-enhanced Raman scattering and surface-enhanced fluorescence dual-mode detection substrates: types, current progress and prospects

Siyu Wang [a], Bowei Li [b,e,*], Jiawen Xiang [b,e], Lianfu Li [a], Shichuan Xi [a], Ruhao Pan [d], Zhendong Luan [c,e], Lingxin Chen [b,e,f,**], Xin Zhang [a,c,e,***]

[a] LaoShan Laboratory, Qingdao, 266237, China
[b] CAS Key Laboratory of Coastal Environmental Processes and Ecological Remediation, Research Center for Coastal Environmental Engineering and Technology, Yantai Institute of Coastal Zone Research, Chinese Academy of Sciences, Yantai, 264003, China
[c] Key Laboratory of Ocean Observation and Forecasting (LOOF), Key Laboratory of Marine Geology and Environment & Center of Deep Sea Research, Institute of Oceanology, Chinese Academy of Sciences, Qingdao, 266071, China
[d] Institute of Physics, Chinese Academy of Sciences, Beijing, 100190, China
[e] University of Chinese Academy of Sciences, Beijing, 101408, China
[f] School of Pharmacy, Binzhou Medical University, Yantai, 264003, China

ARTICLE INFO

Keywords:
Surface-enhanced Raman scattering
Surface-enhanced fluorescence
Dual-mode
Optical sensors

ABSTRACT

Dual-mode optical platforms based on surface-enhanced Raman scattering (SERS) and surface-enhanced fluorescence (SEF) offer the combined advantages of intuitive and fast fluorescence imaging and the multiplexing capability of SERS. They have demonstrated considerable potential in bio-detection and bio-imaging. Herein, two key characteristics of the successful expansion of dual-mode SERS–SEF substrates are reviewed: the morphology and structure of these substrates and the distance effect between molecules and nano-particles. This review summarises the enhancement mechanism, structure, and properties of SERS–SEF substrates, structure and properties of dual-mode SERS–SEF substrates, and their applications in molecular detection, bio-imaging and immuno-assays are discussed. To solve the problem that SERS and SEF have conflicting requirements regarding the distance between reporting molecules and the substrate, a strategy for optimisation of shell thickness to control dual-mode SERS–SEF substrates is proposed. Finally, we expect the dual-mode SERS–SEF technology to be a powerful tool for the analysis of extreme environments by virtue of the protection of their inert shells.

1. Introduction

When a molecule to be measured is placed on a rough metal surface, especially near the gap or tip of metal nano-structures, the electromagnetic (EM) field enhancement due to local surface plasmonic resonance (LSPR) considerably increases the scattering cross-section of the molecule [1–3]. This phenomenon is referred to as surface-enhanced Raman scattering (SERS). Similar to the SERS effect, when dye molecules are placed near nano-metal structures, the intensity of fluorescence emitted by molecules is sometimes enhanced to a certain extent. This phenomenon is commonly known as surface-enhanced fluorescence (SEF) or metal-enhanced fluorescence (MEF) [4,5]. Nearly 50 years have passed since the discovery of SERS and SEF, and nearly 20 years, related research has been receiving increasing research attention (Fig. 1). The enhancement mechanisms of SERS and SEF have been demonstrated after extensive mechanism studies, as described in Section 2 [6–8].

In recent years, with the continuous development and innovation of nano-detection technology, the dual-mode SERS–SEF technology, combining SERS and SEF, has gradually become a promising method for applications in bio-detection and bio-imaging, with fluorescence as a fast indicator and SERS signals used to distinguish specific targets in multiple interactions [9–14]. SERS can identify trace molecules or intermediates and obtain rich structural information. Meanwhile, the quantitative-analysis capability of digital (nano) colloid–enhanced Raman spectroscopy is considerably better than that of standard Raman spectroscopy [15]. However, the requirement of a considerable amount

* Corresponding author. LaoShan Laboratory, Qingdao 266237, China.
** Corresponding author. CAS Key Laboratory of Coastal Environmental Processes and Ecological Remediation, Research Center for Coastal Environmental Engineering and Technology, Yantai Institute of Coastal Zone Research, Chinese Academy of Sciences, Yantai, 264003, China.
*** Corresponding author. LaoShan Laboratory, Qingdao, 266237, China.
E-mail addresses: bwli@yic.ac.cn (B. Li), lxchen@yic.ac.cn (L. Chen), xzhang@qdio.ac.cn (X. Zhang).

https://doi.org/10.1016/j.trac.2025.118353
Received 25 February 2025; Received in revised form 19 June 2025; Accepted 21 June 2025
Available online 23 June 2025

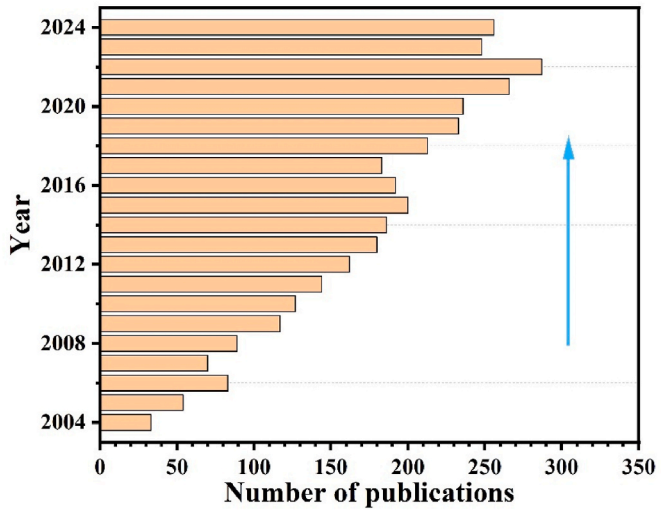

Fig. 1. The number of publications related to SERS and SEF applications has increased year by year since 2004 (Science Direct, available on April 28, 2025).

of acquisition time to obtain reliable data hinders its application in high-speed analysis [6]. In contrast, fluorescence spectroscopy boasts high sensitivity and is capable of swiftly revealing changes in analyte concentrations. Therefore, the SERS and SEF technologies are complementary, and their dual-mode combination offers the advantages of both technologies at once [16]. The integration of these two techniques may serve as an appealing solution across various domains, such as molecular detection, live-cell sensing, tissue diagnostics, protein targeting, drug delivery and in vivo imaging [17–20].

The combination of SERS and SEF is very beneficial for improving the accuracy and sensitivity of detection applications. The exploration of the synergistic effects of SERS and SEF on a same nano-structure is gradually becoming a research hotspot [21–24]. However, because of the conflicting requirements between SERS and SEF in terms of the distance between reporter molecules and the matrix, fluorescent probes require a longer distance to obtain the highest fluorescence enhancement but lose the highest SERS enhancement in doing so [20]. Shell-isolated nano-particles (SHINs) with SERS capabilities not only amplify Raman intensity but also enhance fluorescence intensity, simultaneously circumventing quenching [25]. Consequently, SHINs offer inherent application advantages in SEF [26]. SHINs with thicker coatings may be ideal substrates for SEF, while those with thinner coatings may be more suitable for SERS. The possibility of achieving both SEF and SERS can be achieved by adjusting the coating thickness of SHINs. Therefore, reasonable control of the distance between the reporter molecule or analyte and the metal substrate may solve this problem. With such a structure, nano-probes can generate strong SERS and fluorescence signals. Numerous related studies have fully exploited the synergistic effects of SERS and SEF, which showed remarkable multiplexing detection capability [12,27,28].

In addition, the enhancement of SERS and SEF largely depends on the properties of the nano-structured active substrate, including composition, size, shape, structure, local environment, surface chemistry and interaction with the target molecule [29–32]. Hence, careful design, in-depth exploration and successful fabrication of highly efficient active nano-materials as support substrates is always the key to facilitating the advancement of SERS and SEF technology and wide application thereof. In past few decades, SERS and SEF active nano-materials have undergone extensive development to create more efficient substrates, beginning from the initial nano-sols to solid substrates [5,33,34]. Numerous scholars have made a considerable number of reviews on the materials, applications and mechanisms of SERS and SEF technology, providing us with notable guidance and attracting an increasing number of colleagues to research on detection using SERS or SEF [8,35–39]. However, these remarkable reviews and book chapters were mainly focused on the introduction of either SERS or SEF as a single detection technique. Therefore, with the vigorous development of the dual-mode SERS–SEF detection technology, a complete summary of these problems and latest dual-mode SERS–SEF substrates in this field may be necessary, which can guide researchers of SERS and SEF.

Herein, these dual-mode SERS–SEF substrates are reviewed for better understanding them and their future development (Fig. 2). First, the mechanism of enhancement of SERS and SEF is introduced, and the feasibility of designing dual-mode SERS–SEF substrates is confirmed. Thereafter, the research progress of different types of dual-mode SERS–SEF substrates is introduced, including the application of different material morphologies, structures, sizes and preparation processes. Finally, we discuss current challenges and future prospects with respect to the advancement of SERS and SEF technology in broader fields (such as deep sea, deep space and polar), aiming to reduce the cost of detection in extreme environments. This review may provide valuable reference for the development of dual-mode SERS–SEF substrates, provide guidance and strategy for the design of such substrates with high sensitivity and considerably expand their potential application prospects (e.g. industrial wastewater, deep sea and polar).

2. Outline of the SERS and SEF mechanisms

2.1. SERS mechanisms

After more than 40 years of tireless exploration spanning since the proposal of SERS to now, scientists from various countries have provided many explanations and models for its enhancement and have made continuous amendments and improvements. However, because of the numerous microscopic factors affecting SERS enhancement (such as base configuration, size and material) and their inter-crossing (base–molecule coupling reaction), a complete and reasonable theoretical system has not been formed. Currently, two main enhancement mechanisms of SERS are generally recognised in the academic community: the electro-magnetic enhancement mechanism (EM) and chemical enhancement mechanism (CM) (since the CM is not related to the SEF enhancement mechanism, we will not describe it in detail in this article.) [42–44].

2.1.1. Electromagnetic mechanism

The EM field enhancement effect mainly originates from the interaction between the incident laser with an appropriate wavelength and the local surface plasmon (LSP) on the metal substrate surface, which leads to the sharp enhancement of the local EM field near the nano-metal substrate. Thus, the Raman scattering signal of sample molecules can be improved across a large frequency range, which is conducive to the characterisation and recognition of molecules, even at very low detection limits or at the single-molecule level. Fig. 3a shows the excitation principle of LSPR [40,45]. In addition, the enhanced effect is particularly significant when the frequency of the incident laser matches that of the LSP so as to generate LSPR [46,47]. Meanwhile, this process provides strong EM enhancement around the tip of the nano-structure and also enhances weak light fields near mirrors [48].

The EM field enhancement is achieved by the dual processes of local enhancement and radiation enhancement, including the incident field enhancement factor (EF) provided by the LSPR coupling of incoming radio field and the SERS substrate during excitation, and the emission field EF provided by scattering photons and LSPR coupling during emission [49,50]. In general, the Raman displacement is very small, which leads to the incident enhancement and emission enhancement being close in terms of the order of magnitude. Therefore, in most research works, the Raman EF has been approximated as the fourth square of incident local field enhancement [51]. Tamitake Itoh et al. used cavity quantum electro-dynamics to introduce the EM mechanism

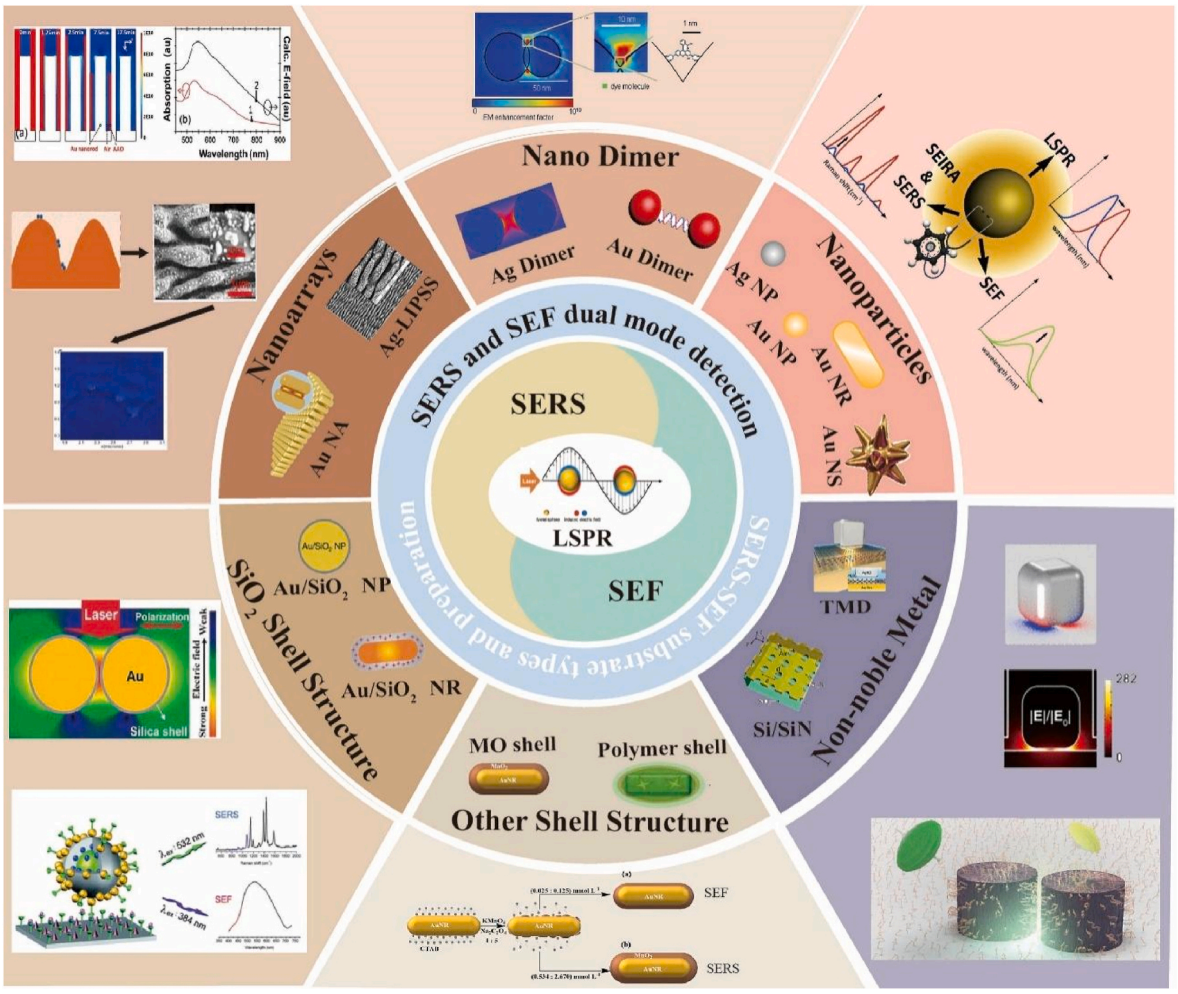

Fig. 2. The type and enhancement mechanism of SERS-SEF dual-mode substrate.

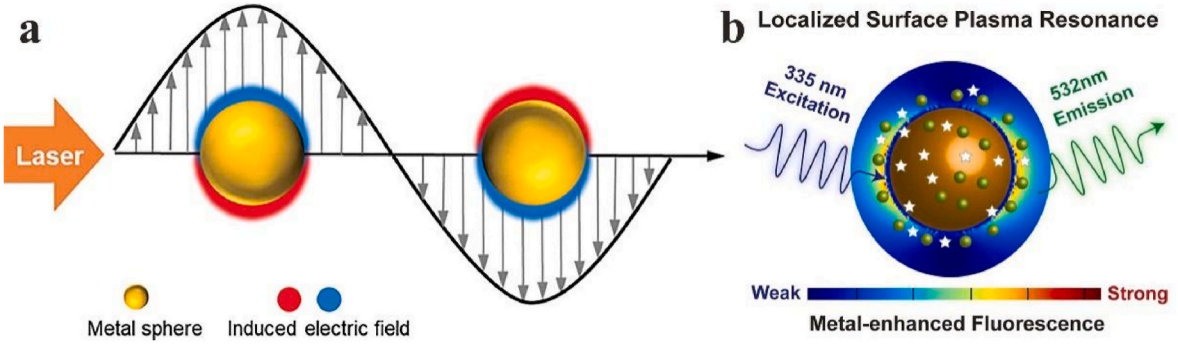

Fig. 3. (a) Schematic diagram for the LSPR of metallic NPs excited by visible light. Reproduced with permission [40]. Copyright 2021, John Wiley & Sons, Ltd. (b) The simplified illustration of SEF. Reproduced with permission [41]. Copyright 2017, Elsevier.

and explained in detail the mechanism of electro-magnetic effects via the method of electro-magnetism [52]. According to current literature reports, the theoretical maximum value of EF of some highly active substrates can reach 10^8–10^{10}, which meets the basic requirements of single-molecule detection, and, thus, the SERS technology can be applied to ultra-sensitive analysis and detection or single-molecule imaging [53,54].

2.1.2. Calculation of SERS enhancement factor (EF_{SERS})

EF is one of the indexes to measure the performance of a SERS substrate. The SERS effect relies on the LSPR generated by metal nanostructures in the near field, which significantly enhances the EM field intensity of the metal surface, thus significantly enhancing the molecular Raman signal. In Raman spectroscopy, after laser is applied to the surface of a substance, the average intensity of the surface electric field intensity can be expressed as $|E|^2 = 2E_0^2 |g|^2$. Considering that molecular dipole oscillation induced by an EM field during the Raman scattering process may enhance the radiation of the dipole, the following expression can be obtained under approximate processing [55]:

$$EF_{SERS} = |E|^2|E'|^2/|E_0|^4 = 4\ |g|^2\ |g'|^2,$$

where EF_{SERS} denotes the EF of the EM field, E′ the electric field that evaluates the scattering frequency. If the Stokes frequency shift is small, g and g' will essentially be in the same wavelength range, following which EF can be re-written as follows:

$$EF_{SERS} \approx 4\ |g|^4 \approx |E|^4/|E_0|^4,$$

In other words, the theoretically calculated value of the SERS EF was proportional to the fourth power of the electric field enhancement, which provided a basis for calculating the EM EF of the SERS substrate via the finite-difference time-domain method later. However, in practical applications, researchers usually express the enhancer EF [56] as follows:

$$EF = (I_{SERS}/N_{Raman})/(I_{Raman}/N_{SERS}),$$

where I_{SERS} and I_{Raman} denote the intensities of probe molecules in the SERS spectrum and Raman spectrum, respectively. The ratio I_{SERS}/I_{Raman} can be experimentally measured. N_{SERS} and N_{Raman} denote the number of analyte molecules in the region of excitation-light irradiation on the SERS substrate and ordinary substrate, respectively. The value of N (N_{SERS} and N_{Raman}) can be calculated as follows:

$$N = ((N_A \times M \times V_{solution})/S_{sub}) \times S_{laser},$$

where N_A denotes Avogadro's constant, M the molar concentration of the solution, $V_{solution}$ the volume of the probe molecular solution, S_{sub} the area of the probe molecular solution on the substrate and S_{laser} the area of the laser spot; the N_{SERS}/N_{Raman} ratio is experimentally measured. In summary, the EF of the basis is calculated.

2.2. SEF mechanisms

Upon positioning a fluorophore either on the surface of a conductive metal or in proximity to its neighbouring particles, the quantum yield is enhanced, concurrently reducing the fluorescence lifetime. This combined outcome of elevated quantum yield and diminished fluorescence lifetime is collectively denoted as MEF (or SEF) [57,58]. This effect was first discovered by Drexhage in the late 1960s, when he was studying fluorescence lifetime in the presence of metal films [59,60]. The mechanism of the enhancement of the SEF effect is shown in Fig. 3b [41]. When incident light is irradiated on the metal nano-structure, the coupling of LSPR and incident field near the substrate results in massive enhancement of local EM field, which can effectively improve the absorption of molecules. Therefore, the molecular radiation is considerably enhanced compared with that in a vacuum, resulting in a high-sensitivity SEF effect [61]. Different from SERS, the fluorescence process is also affected by the quantum yield; therefore, in SEF, it is usually required that a certain distance should be maintained between molecules and the metal surface to avoid fluorescence quenching.

Similar to SERS, EF of the EM field is also a major factor to measure the effect size of SEF [62]. The results reported by Guerrero's group demonstrated that the SEF effect is generally proportional to the square of the field enhancement, wherein the enhancement is entirely caused by the excitation enhancement brought about by the amplification of the EM field [63]. With the gradual deepening of research, it has been observed that both the excitation and radiation processes should be considered to comprehend the SEF effect [64]. For the excitation enhancement process, the incident light field was coupled with the base LSPR to obtain the incident EF, which was similar to the excitation mechanism of SERS and could considerably improve the excitation efficiency of fluorescence. Thus, based on the similarity of SERS and SEF in EM, theoretical support for the construction of a dual-function platform can be provided. Moreover, several studies have demonstrated that SEF is predominantly governed by the energy transfer occurring between the molecules and the silver surface. And the greater spatial fluctuations observed in the SEF signal imply a more intricate behavior of the molecules in the vicinity of the silver surface [65,66].

In addition, the enhancement mechanism of SEF is also partly caused by non-radiative coupling. Simply speaking, the non-radiative coupling between the dye molecule and the metal nano-structure can facilitate more efficient transfer of the excited state energy of the dye molecule into the plasma mode of the metal nano-structure [64,67]. This energy transfer process can significantly enhance the fluorescence signal. However, the emission enhancement process is also closely related to the quantum yield of the emitted light field of the molecule, which depends on the simultaneous influence of the radiative transition caused by photon emission and the non-radiative transition caused by loss in the surrounding environment. Theoretical and experimental studies have shown that the material of the substrate, the geometric configuration and the selection of incident light play a decisive role in the enhancement or quenching of molecular fluorescence [62,68].

2.2.1. Calculation of SEF enhancement factor (EF_{SEF})

EF is also one of the indicators to measure SEF performance. The EF of SEF is usually expressed in the [69] following simple formula:

$$EF = I_{SEF}/I_{Normal},$$

where I_{SEF} denotes the fluorescence intensity of the molecule to be tested on the SEF substrate and I_{Normal} that of the molecule to be tested on the pure glass substrate.

3. Research status of SERS-SEF dual mode substrate

Because of the simplicity and low cost of preparation, a noble metal nano-sol was the most used SERS substrate in the early stage. Under the influence of excitation by visible light and near-infrared light, gold (Au), silver (Ag) and copper (Cu) exhibited remarkable properties as SERS substrates. Of these, Au and Ag NPs were more widely used in SERS applications because of their high SERS enhancement properties. For Au and Ag NPs, the LSP formant is usually located at ~520 and ~400 nm [70]. Common spherical NPs can be prepared via chemical reduction and laser ablation [71]. In the context of SEF sensing within a solution, the dimensions of colloidal NPs play a crucial role [1]. For diminutive metallic NPs, light absorption predominates over scattering, and the quenching of fluorophore emission tends to overshadow its enhancement. Consequently, there is a preference for larger NPs and geometries that exhibit increased scattering cross-sectional areas [72]. In SERS and SEF, the distances of both of molecules involved in SEF near the metal surface and those involved in SERS from the metal surface affect their spatial distribution and local viscosity and also the intensity of the enhanced EM field [73]. In addition, the aggregation state of metal particles and the spacing between the metal structure and the emitter also exert a strong influence on the enhancement rate of each of SERS and SEF properties [67]. Therefore, reasonable design of the shape and structure of metal particles can result in a dual-functional SERS–SEF substrate with remarkable properties. Table 1 includes the main research progress since the development of SEF-SERS dual mode substrate, including the performance and analytical figures of merit of this method (see Table 2).

3.1. SERS-SEF sensors based on noble metal substrate

SERS and SEF provide important means for the detection and characterisation of the structure of nano-scale samples, and a high-quality active substrate is the basis and key to the realisation of these two technologies [90]. Ever since the emergence of SERS and SEF, various nano-structures made of precious metal nano-materials are still the most favoured by scientists worldwide. For example, spherical NPs of Au, Ag and Cu have been used as substrates with strong activity in the visible light band [91,92] for a variety of practical detection applications because of their high sensitivity, fast preparation, simple operation and low cost. Simultaneously, more SERS hotspots have been added through

Table 1
Composition of different types of SEF-SERS bimodal substrates, synthesis methods and their enhancement factor (EF) (The "/" does not mean there is no enhanced performance, but the relevant data is not provided in the citation).

Type	Substrates	Synthesis method	Molecules	EF_{SERS}	EF_{SEF}	Ref.
Au/Ag NPs	Au NPs	Evaporation/sputtering techniques	Rh B	10^2 (Evaporation/sputtering)	100 (Evaporation/sputtering)	[74]
	Au NPs film	DC sputtering	Crystal violet (CV)	6.17 (in SiO_2/Si Substrates)	5.8 (in SiO_2/Si Substrates)	[75]
	Ag Island membrane	Z-deposition	HPDR13	10^4	50	[76]
	Ag-LB azopolymer films	Mixed LB film technique	Bis(phenethylimido) perylene	10^4	100	[77]
Au/Ag dimer	Ag NPs dimer	Solution sol method	R6G	~10^4 (Theoretical EM)	~10^4 (Theoretical EM)	[78]
	Au NP dimers	DNA-directed self-assembled	ATTO647 N	/	119	[79]
	AuNP-chains	DNA origami as the template induced dimers nanostructures	4-MBA	5.3 (AuNP-chains/Au NP dimers)	/	[80]
Ag/Au Nanoarrays	Ag fractals	Electrochemical method	MG and PATP	8.1×10^6	6	[81]
	Au nanoprisms arrays	Electron-beam lithography	4-NTP	$10^{5.2}$	$10^{2.6}$	[82]
	Ag nanolayered structure	LIPSS technology	CV	7.85×10^5	14.32	[73]
	Ag nanolayered structure/Si	LIPSS technology	R6G	2.11×10^6	24.83	[9]
SiO_2 Shell Structure	Ag film/SiO (or SiO_2)	Varying dielectric thickness	P-PTCO	/	10	[83]
	Au@SiO_2 dimers	Theoretical model	Analogue simulation	10^9	10^4	[84]
	Ag@SiO_2	Theoretical model	Analogue simulation	10^9	10^4	[85]
	Ag@SiO_2 nanoparticle	Solution sol method	PATP and DMAB	10^3	3.6	[11]
Other Shell Structure	Au@$(PAH\text{-}PAA)_2$-1@Ag	Layer-by-layer assembly	Toluidine Blue O	3.0×10^5	25.6	[64]
	Ag NR@DTNB@PAH@PAA	Solution sol method and Layer-by-layer assembly	DTNB and Alexa Fluor 647	5.76×10^6	25.54	[12]
	Au NR@MnO_2	Solution sol method	Cyanine dye IR-820	6.7	34.5	[86]
Non-noble Metal	Monolayer $MoSe_2$-coupled plasmonic nanocavors	Annealing and ultrasonic method	Monolayer $MoSe_2$	10^7	6000	[87]
	Silicon nanodimers	Inductively coupled reactive ion etching-Chemical Etching-Electron beam lithography-Cr etching	β-carotenal	1720	470	[88]
	Silicon nitride	Plasmonic-enhanced chemical vapour deposition	R6G and CV	10^3	10^3	[89]

Table 2
Comparing the advantages vs. disadvantages of the dual detection mode vs. traditional detection mode.

Comparison dimension	Dual Detection Mode	Traditional Detection Mode
Sensitivity	High, capable of detecting low-concentration targets	Lower, suitable for high-concentration detection
Selectivity	Low, suitable for trace analysis	Higher, preconcentration may be required
Limit of detection	High, good specificity	General, may be subject to interference
Operational complexity	Higher, requires specialized equipment and training	Lower, easy to operate
Cost	High, expensive equipment and reagents	Low, suitable for resource-limited laboratories
Portability	Low, large equipment size	High, suitable for field detection
Scope of application	Biomedical, environmental monitoring	Environmental monitoring, industrial detection
Data processing	Complex, requires specialized software	Simple, manual analysis is sufficient

various substrate configurations, such as nano-rods (NRs), nano-petals, nano-cubes, nano-stars and other structures successively appearing in recent years, which have considerably improved the detection sensitivity of SERS [93,94].

3.1.1. SERS-SEF sensors based on Ag or Au NPs substrate

In both SERS and SEF, the EM enhancement originates from the LSPs on the surface of metal NPs. Hence, the fabrication of metal nano-structured substrates using chemical or physical approaches is indispensable. Tang et al. prepared porous Au NPs films with different densities and sizes by changing the deposition time and hot annealing treatment and confirmed the presence of the optimal shape and size of Au NPs corresponding to the maximum SERS and SEF effect [74]. Merlen et al. used evaporation and sputtering techniques to prepare nano-structured Au surfaces on silicon and glass surfaces, respectively, and observed that the fluorescence signal of Rhodamine 6G (R6G) was super-imposed on the SERS signal, indicating that the observed enhanced Raman signal and fluorescence signal may have had a common source [21]. Similarly, by studying the SEF and SERS of Au NP films deposited on Si and SiO_2 substrates, Chai et al. proved that the fluorescence peak intensity of different substrates similarly varied with Raman intensity [75]. Therefore, the two processes of SEF and SERS have similar enhancement and photo-bleaching mechanisms, the contribution of the electron resonance effect to the enhanced signal strength of certain dye molecules deposited on the rough Au surface. The combination of EM enhancement and electron resonance effect produces a stronger signal, because of which even a very small number of molecules (such as monolayer molecules) can be detected.

The Langmuir–Blodgett (LB) technique provides an accurate method for controlling film thickness and surface uniformity. An LB films exhibit strong fluorescence because of the spatial limitations of its structure; therefore, effective SERS and SEF effects can be obtained on the surface of LB film–coated Ag NPs. Constantino et al. documented the localised mapping and comprehensive imagery of SERRS spectra pertaining to a bis(benzimidazole) perylene (AzoPTCD) LB monolayer situated on a Ag island film. They noted the manifestation of SEF emanating from excimer formations within LB film aggregates [95]. The emergence of SERRS and SEF patterns could be clearly observed, indicating that the orientation of the packaged AzoPTCD chromophore on the metal surface was edged-opposite or right-opposite, rather than flat (Fig. 4a). They then investigated the photo-isomerisation of a Ag island film coated with a methacrylic acid homoperic LB film by means of SERS and SEF spectra. According to the experimental results, the enhancement factor of SEF

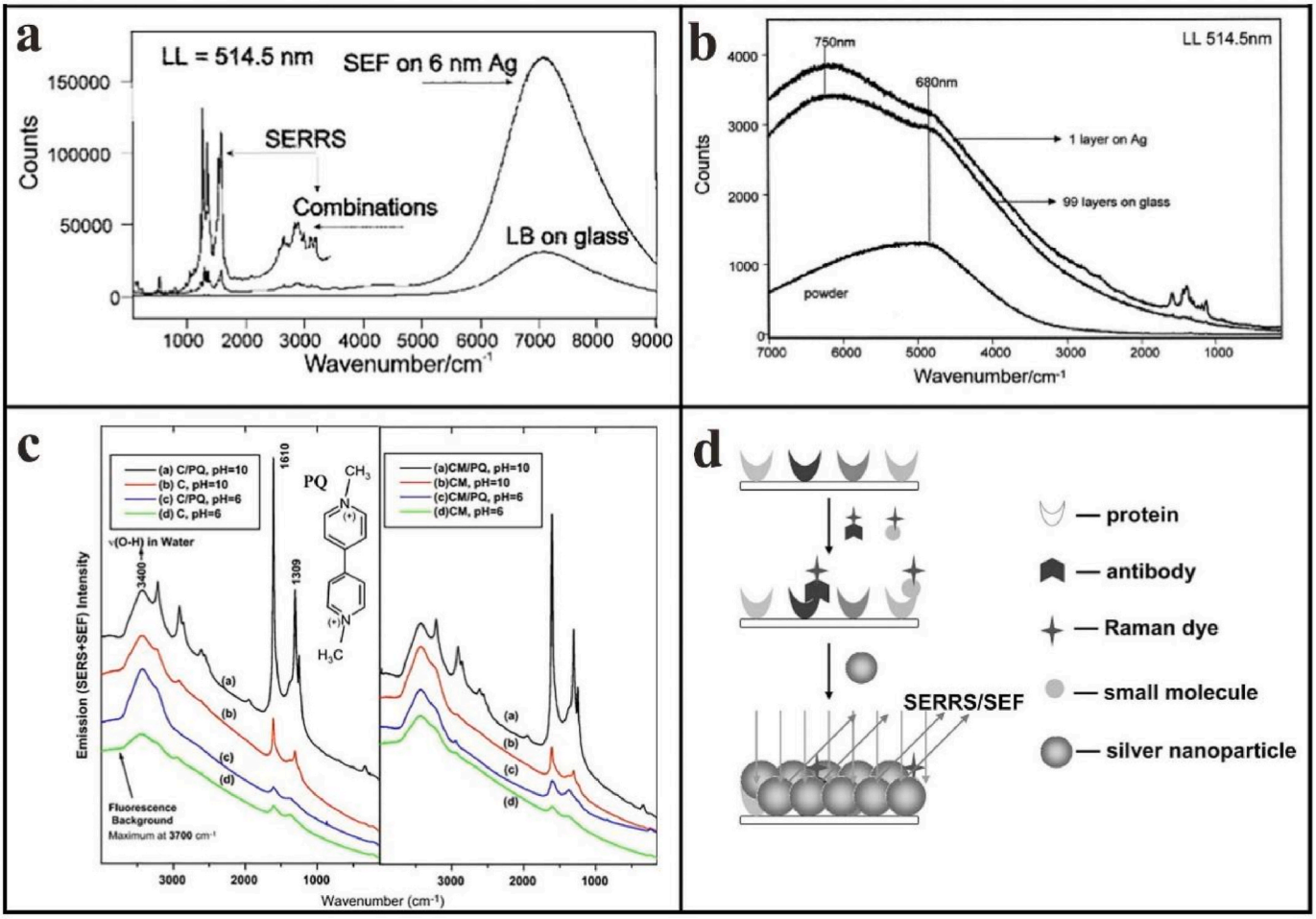

Fig. 4. (a) Features the SERRS and SEF characteristics of an Azo-PTCD LB monolayer. Reproduced with permission [95]. Copyright 2000, John Wiley & Sons, Ltd. (b) RRS, SERRS and SEF spectra of HPDR13 on a Ag island monolayer. Reproduced with permission [76]. Copyright 2001, Elsevier. (c) Emission SERS and SEF (superposition) spectra of different samples and their PQ complexes. Reproduced with permission [96]. Copyright 2011, Elsevier. (d) Schematic diagram of protein-ligand SERRS/SEF dual-mode detection scheme. Reproduced with permission [97]. Copyright 2008, American Chemical Society.

was at least 99 and that of SERS was ~10^4 (Fig. 4b) [76]. Aroca et al. prepared an LB monolayer of diphenyl ethyl amino perylene on a Ag island membrane substrate; studied its SERS, SERS and SEF spectra; and obtained the map of the SERS/SERRS signal and global Raman image at a specific vibration wave number [77].

At low concentrations, SEF can significantly improve the sensitivity and light stability of fluorescence-based detection. Moreover, because of the elimination of self-quenching and photo-bleaching between chromophores, SERS can compensate for the shortcomings of fluorescence in terms of light stability; therefore, the combined technology of SERS and SEF has a potential application value in ultra-sensitive analysis. Guo et al. described a technique for improving SYBR Green I detection by means of SERS and SEF using Ag NPs with an average size of ~70 nm [10]. Roldan et al. used Ag NPs to conduct SERS and SEF detection on paraquat and humic acid both extracted from soil improved for >30 years using crop straw, cow pulp and cow dung. They studied the interaction mechanism between paraquat and humic acid and observed the correlation between this interaction and the structural changes of humic acid caused by different modifiers in the soil (Fig. 4c) [96]. Han et al. assembled Ag NPs onto protein–ligand complexes through covalent and non-covalent binding, thus forming Ag aggregates with SERS and SEF double activity so as to reliably determine functional proteins (Fig. 4d) [97].

3.1.2. SERS-SEF sensors based on Ag or Au Dimer substrate

Dimers of NPs are an effective tool to study the complex spectral variation of plasmon resonance in SERRS and SEF processes. Itoh et al. used Ag NP dimers to analyse the intensity and spectral instability of R6G molecules under scintillation and EM mechanisms in SERRS and SEF (Fig. 5a) [98]. Meanwhile, Itoh et al. experimentally observed the spectral changes of SERRS and SEF for single dye molecules adsorbed on a single Ag NP dimer under strong coupling conditions [78]. Considering the shift from ultra-fast SEF to its conventional form, the calculated enhancement and quenching coefficients effectively mirrored the empirical spectra of SERRS and SEF.

In addition, the DNA nano-technology strategy is a promising candidate material for SERS and SEF, which can pinpoint the gaps of NPs towards achieving enhanced SERS or SEF [99]. In the early stage, Acuna et al. commenced a seminal investigation featuring the attachment of one or two Au NPs to DNA origami pillars, with individual fluorescent dyes positioned in proximity to Au NP monomers and dimers varying in size [79]. The researchers examined the manner in which the fluorescence intensity and lifetime of individual dyes varied for different nano-assemblies, achieving a fluorescence enhancement of up to 117 times for Au NP dimers (Fig. 5b). The variation mechanism of electric field intensity of the monomers and dimers of Au NPs with particle size of 80 nm and particle spacing of 23 nm was investigated. It was discovered that the enhancement in fluorescence brightness originated from the significantly intensified local EM field generated by plasmonic

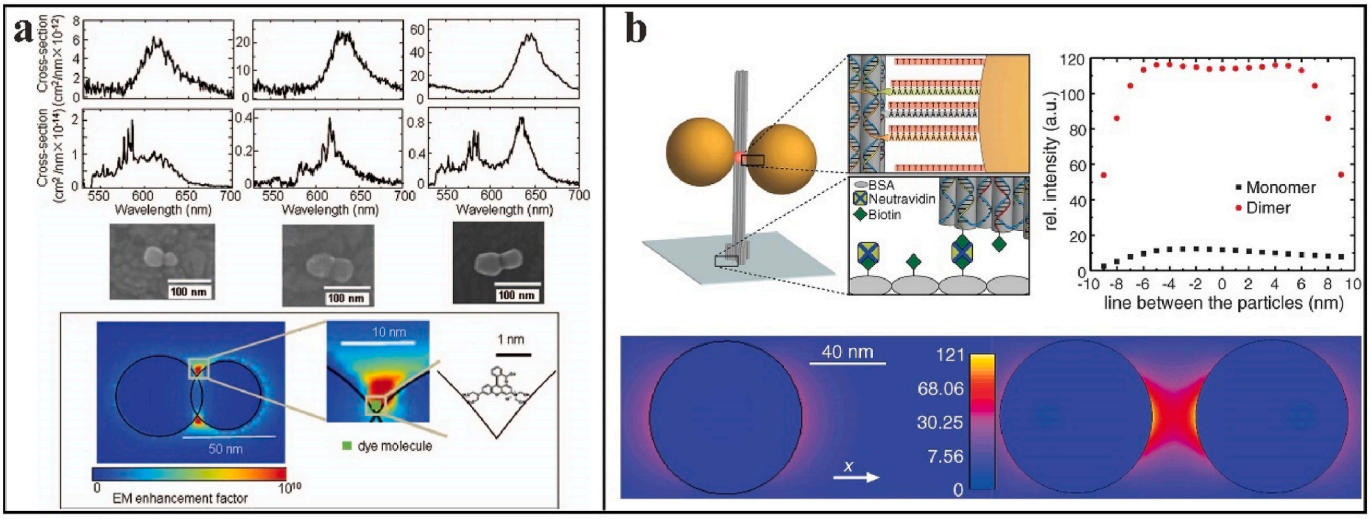

Fig. 5. (a) The Ag NP dimer/R6G plasmon resonance spectra, SERRS and SEF, and SEM images of three Ag dimers. Model of SERRS generation by Ag dimer: Calculation of electric field distribution around Ag dimer by FDTD method. Reproduced with permission [98]. Copyright 2012, American Scientific Publishers. (b) DNA origami column diagram of Au NPs dimer (top) and numerical simulation of electric field strength of the dimer (right). Reproduced with permission [79]. Copyright 2012, Science.

nano-structures, and this enhancement was contingent upon excitation conditions and the influence on the radiative and non-radiative decay rates of the fluorescent dye. Zhao et al. employed supplementary DNA splicing techniques to assemble DNA-guided Au NP dimers into nano-ribbon structures, demonstrating a substantial amplification in SERS signals both from Au NP dimers and chains [80]. However, the applicability of NP dimers induced by DNA nano-technology in SERS–SEF dual-mode-detection remains to be further investigated.

3.1.3. SERS-SEF sensors based on Ag or Au Nanoarrays substrate

The characteristics of plasmonically active nano-structures are contingent upon variables including dimensions, morphology and surrounding dielectric medium [100]. Nano-structures with particular configurations in plasmonic materials are of significant interest across a range of applications aimed at enhancing fluorescence through transduction mechanisms. Periodic metal NP arrays can generate LSPRs. The modulation of the NP spacing ratio or the diameter of the NP affects LSPR, and metal nano-structures with anisotropic symmetry, such as NRs, can produce LSPRs with high quality factors [101–104]. NRs can be designed to control their particle characteristics, including shape, length, width and inter-particle coupling. Analogous to the amplification of molecular Raman scattering, the excitation of LSPRs on plasmonic metal nano-structures can intensify the fluorescence signal emanating from proximate fluorophores, a phenomenon termed SEF [105]. SEF is effective when the fluorophore resides within an optimal proximity to the metal surface, facilitating enhanced emission efficiency, diminished photo-bleaching rates and bolstered photo-stability of fluorophores. The concurrent study of SERS and SEF holds significant promise for sensor development, rendering them particularly appealing for such applications [81].

A significant challenge in the practical application of SERS and SEF lies in fabricating a substrate capable of consistently enhancing signals from the probe molecules uniformly across its surface and maintaining this enhancement across different substrates. This problem originates from the presence of hot spots, that is, small, randomly distributed regions with significant electric field strengths, resulting in a significant increase in SERS/SEF signals. Such hot spots usually occur when solution-formed NPs are applied to the surface of nano-structures; fabricating a substrate in this manner usually produces NPs in random locations, resulting in hot spots. One way to address this issue involves the fabrication of precisely arranged arrays of nano-scale metallic constructs [106]. This method allows for the regulation of the emergence and placement of hot spots on the substrate. Arrays of metal NRs with consistent diameters and placements establish a foundation for reliable SERS and SEF. Damm et al. investigated the SEF and SERS characteristics of freestanding Au nano-rod arrays embedded within a porous alumina template (AAO) [100,107,108]. An inverse correlation between SEF and SERS was discerned by modulating the thickness of the AAO matrix. Wang et al. took a cicada wing as a template, and the nano-gap between adjacent conical protrudates could be effectively controlled by adjusting the sputtering time [109]. Upon optimising the substrate, it was observed that the Ag NP@Ag@cicada array significantly enhanced the SERS signal and provided a certain SEF enhancement effect. The Ag NP@Ag@cicada remarkable optical properties indicated that it had considerable potential in label-free detection and bio-analyte determination.

Fractal-like nano-structures have attracted increasing attention both experimentally and theoretically. Typically, Dong et al. used an electrochemical reduction method to prepare an effective, reinforced substrate with a fractal nano-structure using Ag NP clusters as raw materials [81]. The substrate prepared allowed for the concurrent detection of surface-enhanced spectra of R6G molecules, encompassing both SERRS and SEF. The findings indicated the generation of a potent EM field within the Ag fractal nano-structure upon laser irradiation (Fig. 6a). This demonstrated the efficacy of the fractal-like substrate in amplifying both Raman and fluorescence signals, thereby affording the substrate with dual capabilities for signal enhancement in these modalities. Wallace et al. engineered a range of metallic configurations, which included super-imposed arrays of Au nano-caprisms, demonstrating the potential for SERS, SEF and surface-enhanced infrared absorption (SEIRA) [82]. The hexagonal lattice consisted of a smaller prism for SERS and SEF applications (prism base length 0.25 μm) and a larger triangle for SEIRA purposes (base size 1–2 μm). Fig. 6b shows the scattering images of Fischer patterns of different sizes and their SEF images. The SEF images of the superimposed patterns (G−H) demonstrate the effect of superimposing small and large triangles. It can be observed that the SEF signal is not only present at the edges of the large triangles but also at the intersections between the small and large triangles. This indicates that the superimposed structures can create new enhanced regions, thereby further increasing the fluorescence signal. Fig. 6c displays the SERS images of Fischer patterns of different sizes. The SERS images of the superimposed patterns also show significant SERS enhancement, with

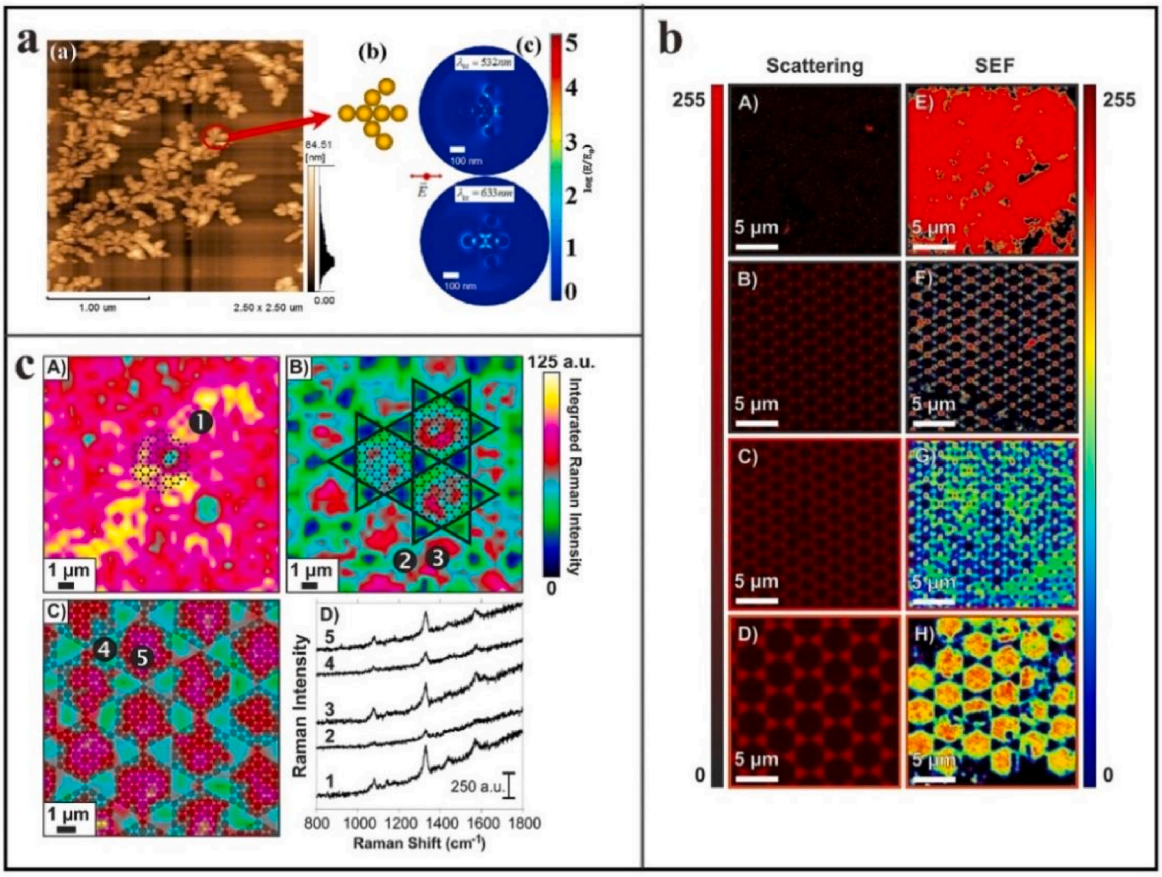

Fig. 6. (a) AFM images of Ag fractal nanostructures, simulation models of fractal nanostructures and electric field distribution. Reproduced with permission [81]. Copyright 2014, Elsevier. (b) Scattering and SEF of Fischer's patterns of different sizes with superimposed patterns; (c) Composite SERS mappings from 1300 to 1350 cm^{-1} for patterns functionalized with 4-NTP, exhibiting various lateral dimensions. Reproduced with permission [82]. Copyright 2016, American Chemical Society.

the signal primarily concentrated at the intersections between the small and large triangles. This further confirms the advantage of superimposed structures in enhancing the Raman signal. The super-imposed design exhibited areas conducive to SEF, SERS and SEIRA, thereby presenting auspicious prospects for the multi-spectral sensing of molecules (Fig. 6b and c). Zhang et al. used the discrete dipole approximation method to study the local electric field enhancement of overlapping Ag triangle nano-sheets [110]. For double-layer Ag triangle nano-sheets, with increase in thickness, the electric field enhancement gradually shifted from the corner near the gap to the centre of the gap and the electric field intensity gradually increased. The maximum 'hot spot volume' was observed upon increasing the thickness to 20 nm. Their study confirmed that overlapping Ag triangular nano-plates had considerable potential in SERS and SEF detection.

The laser-induced periodic surface structure (LIPSS) technique is a direct method for rapid, low-cost nano-structure formation. Quasi-periodic nano-ripples can be formed on semi-conductor and metal surfaces by correctly selecting the repetition rate, the energy density of the ultra-fast laser and the scanning speed [73]. The direction of beam polarisation and the wavelength of the radiation affect the direction and period of nano-structures formed. This configuration may mitigate the aggregation of metallic NPs. Moreover, the amalgamation of SERS and SEF within a singular bi-metallic substrate may enhance the acuity and consistency of detection, which is particularly beneficial in bio-medical research. In the production of LIPSS-based SERS substrates, the most common method is to deposit via vacuum deposition a thin film of Au or Ag on a rough surface. Tang et al. sputtered Ag nano-films on a pre-strained flat polydimethylsiloxane (PDMS) substrate, and they formed Ag folds and triangular cross-sectional structures with different sizes and periodicity by releasing the PDMS substrate [34]. Utilising these structures as ultra-sensitive bio-chemical sensing probes for SEF and SERS analyses facilitated the detection of exceedingly low concentrations of crystal violet (CV) and R6G, reaching down to 10^{-14} M. Lu et al. developed a SERS–SEF dual-mode hierarchical structure on a single biometrical substrate using LIPSS. The hierarchical structure consisted of micro-grooves, NPs and nano-ripples (Fig. 7) [73]. Upon employing CV as the indicator molecule, the intensities of both Raman and fluorescence signals amplified owing to the dual-mode SERS–SEF effect, with the EFs recorded at 7.85×10^5 for Raman and 14.32 for fluorescence. Furthermore, Lu and colleagues accomplished swift dual-mode-detection of glucose by fabricating controlled, hierarchical LIPSS on silicon substrates, which were integrated with substrates conducive to both SERS and SEF [9]. The enhancements achieved through SERS and SEF were as high as 2.11×10^6 and 24.83, respectively. Moreover, the results of clinical validation of dual-mode glucose detection in human blood samples correlated well with established clinical data, indicating promising application potential.

Notably, noble metal substrates (such as those of Au and Ag) are associated with high preparation costs, mainly because of the expensive materials and the complex equipment and processes required by some preparation methods (such as electron beam lithography and chemical vapour deposition). However, noble metals have good chemical stability and are not easily oxidised or corroded, making them suitable for various environmental conditions. Although the preparation process has high requirements for experimental conditions, leading to moderate reproducibility between different batches, their detection sensitivity is high, capable of achieving single-molecule detection, with SERS EFs reaching $>10^6$ and SEF EFs reaching $>10^2$. They are suitable for high-

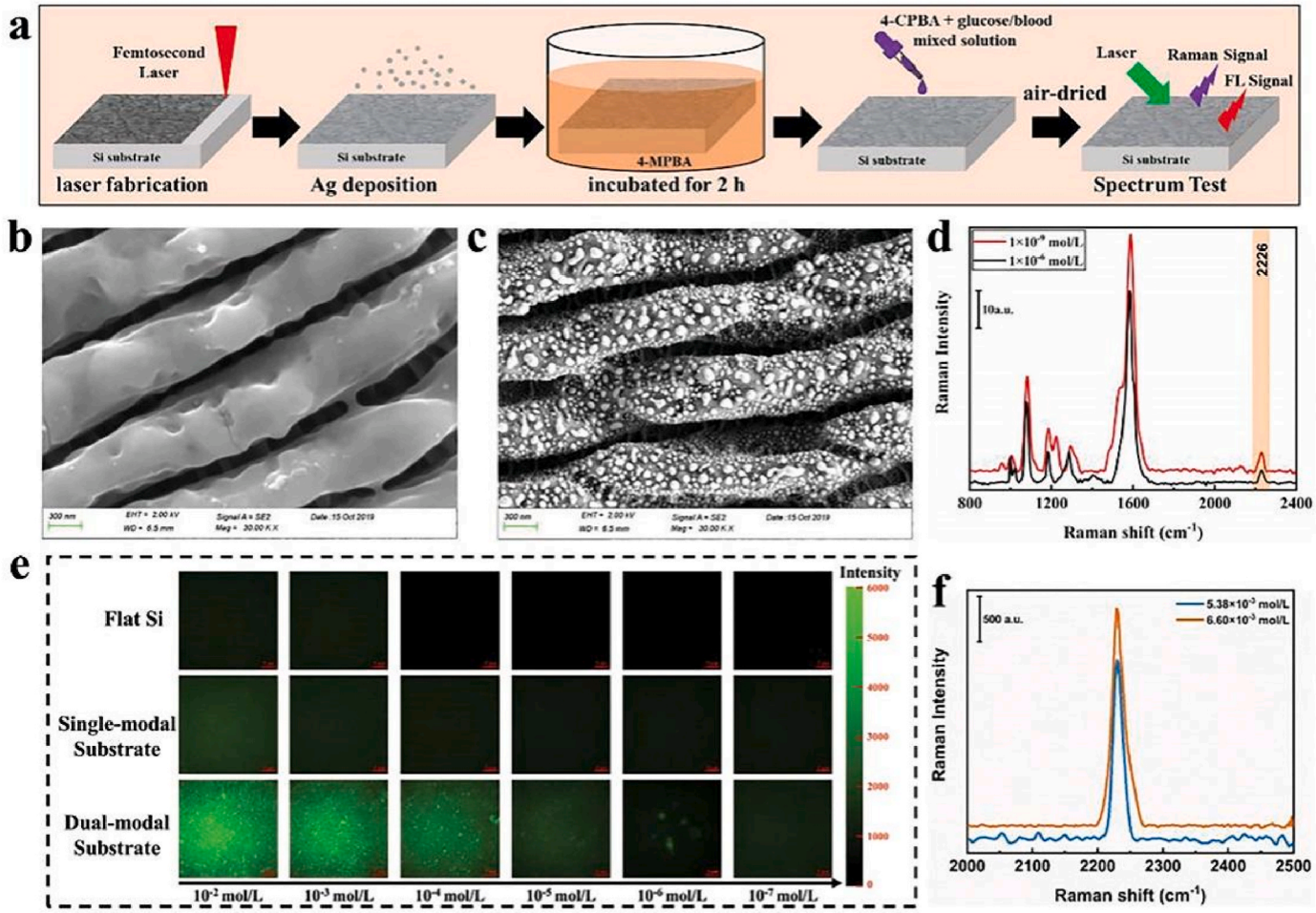

Fig. 7. a) Diagrammatic representation of the glucose sensing protocol. (b) Photomicrograph of the single-mode SERS system. (c) Photomicrograph of the dual-mode SERS-SEF system. (d) Detection limits for glucose using a single SERS substrate (indicated by the black line) and a dual-mode SERS-SEF substrate (indicated by the red line). (e) Fluorescence mapping of glucose on various platforms with glucose concentrations spanning from 10^{-2} to 10^{-7} mol L^{-1}. (f) SERS spectra of glucose in clinical human blood samples at concentrations of 5.38×10^{-3} and 6.60×10^{-3} M. Reproduced with permission [9]. Copyright 2012, John Wiley & Sons, Ltd. (For interpretation of the references to colour in this figure legend, the reader is referred to the Web version of this article.)

sensitivity detection and applications in complex environments.

3.2. SERS-SEF sensors based on core-shell structure substrate

The application of pure metal substrates also has inherent problems; for example, the direct contact between metal NPs and analyte molecules and environmental media leads to unnecessary CT, which affects the detection result. Moreover, metal NPs are unstable and easily aggregate, which is not conducive to repetitive detection and long-term storage [110,111]. Their bio-compatibility and test effect under high temperature conditions are also poor. In addition, in the SERS effect, the enhancement effect monotonically decreased with increase in the distance between dye and metal NPs, while the emission of the fluorophore was quenched when its distance from the surface of NPs was very low (approximately <10 nm). Therefore, the maximum SEF effect can be achieved via the ideal minimum distance between the fluorophore and metal NPs. Aiming at overcoming these shortcomings, the outer layer of metal NPs can be wrapped with a thin shell of a transition metal or an insulating material with controllable thickness so as to avoid the direct contact between the core and detection molecules or interference from environmental impurities, following which the long-term EM field enhancement from the metal core can be effectively transmitted to form a stable core–shell nano-structure substrate for detection [112]. Meanwhile, researchers were able to adjust parameters such as material, size and thickness of the kernel or shell, thus further improving the enhancement effect and application range of SERS and SEF [113,114]. The versatility of core-shell nanostructured substrate greatly expands the applicable research field of SERS and SEF technology, and is expected to play an important role in high-energy materials, pathological diagnosis, biological analysis and environmental pollution detection.

SHIN-enhanced Raman spectroscopy (SHINERS), a technique designed by Professor Tian's team, replaces the tip of a Au probe with a single layer of Au NPs coated with an ultra-thin shell of silica or alumina so as to extend the substrate and improve SERS activity on the substrate [112,115,116]. The main advantages of this shell isolation mode are its higher detection sensitivity, and also it has a wide range of practical applications for various morphologies of materials. For SHINERS, the ultra-thin shell is essential to expose the adsorbent to the maximum EM field emanating from the Au core. However, for a fluorophore located on the enhanced nano-structure, increase in thickness would result in a continuous transition from fluorescence quenching to fluorescence enhancement [6].

3.2.1. SERS-SEF sensors based on SiO_2 shell structure substrate

The core-shell structure of Au and Ag NPs coated with SiO_2 (such as Au@SiO_2 and Ag@SiO_2) is a typical feature in the SHINERS approach [112,117]. SiO_2 shell have remarkable adjustability vis-à-vis size and thickness, and these SHINs can be used to enhance both the Raman signal and fluorescence signal by properly controlling the shell thickness [63]. Initially, Initially, Tarcha et al. observed SEF and SERS on active

6-, 10- and 14-nm Ag films coated with SiO_2 [83], and they obtained similar results with 6-nm Ag films coated with 6-nm SiO. The SEF work was performed on fluorescent molecules with different quantum yields, and the typical EF of the fluorescence signal obtained was ~10. Both SiO_2 and SiO coatings provided a stable surface with clear hydrophilicity. This stable structure was suitable for the development of conventional analytical techniques for SERS and SEF as biological and chemical sensors. Pei et al. used the three-dimensional (3D) finite element method (3D-FEM) to study and analyse EM enhancement, quantum yield and Raman and fluorescence enhancements of Au@SiO_2 dimers with different nuclear radii and shell thicknesses [84]. The results demonstrated that the SERS effect was closely related to EM enhancement, while the SEF effect mainly depended on the competition between EM enhancement and fluorescence quantum yield, both of which could be modulated by nuclear radius, dimer distance and shell thickness. Wei et al. also used three-dimensional finite element method to confirm that SiO_2 shells can effectively transmit strong EM enhancement of Ag nuclei, and the fluorescence enhancement effect is better than that of uncoated Ag dimers [85].

With the continuous development of SHINERS applications in SEF, many bifunctional particles have been developed to take advantage of the advantages of SERS and SEF as detection tags [6,19]. The combined signal of SERS and fluorescence spectra, instead of the separate optical signal, can provide a wider spectral range, so as to achieve effective coding [118]. Zhou et al. demonstrated a method for preparing Au-core-Ag shell NPs that display both SERS and SEF activity by embedding dye molecules between the core and shell [64]. A poly-electrolyte (PE) was used to adjust the spacing between the core and shell and the dye position. Multi-layer PE deposition is an effective and flexible method for introducing various types of dye molecules into nano-structures. Chang et al. synthesised composite NPs with specific morphologies, such as the Ag@SiO_2 core–shell structure or Ag@SiO_2/Ag satellite structure, through a well-controlled single-pot reaction in a micro-emulsion medium [67], and they coded various dyes as reservoir tracers into these composite NPs (Fig. 8a). Notably, this satellite structure can be used to obtain composite SERS-SEF NPs via hydrophilic/hydrophobic modification of dye molecules and adsorption of dye molecules at different distances in the core. Wang et al. proposed the SERS–fluorescence joint spectral encoding method, a new optical coding method, using organic metal–quantum dot mixed NPs (OMQ NPs) with nano-layered structures [118]. By coupling different encoded antibodies to different encoded OMQ NPs, the potential application of this coding system in high-throughput detection was investigated by multi-sandwich immunoassay (Fig. 8b).

The analysis technology using SERS fluorescence dual-mode nanoprobes is expected to become a powerful tool for biological detection and biological imaging, and has a broad application prospect in the biomedical field. The maximum strength of SEF was obtained by using a silicon shell spacer of about 9 nm. Zhang et al. used a dual-function nanostructured Ag@SiO_2 NP modified with p-aminothiophene (PATP) -coated quantum dots (QD) for simultaneous immunoassay of surface-enhanced Raman scattering (SERS) and surface-enhanced fluorescence (SEF) (Fig. 8c) [11]. Lee et al. used highly stable silica coated Au NPs to design a simultaneous SERS fluorescence imaging technique for

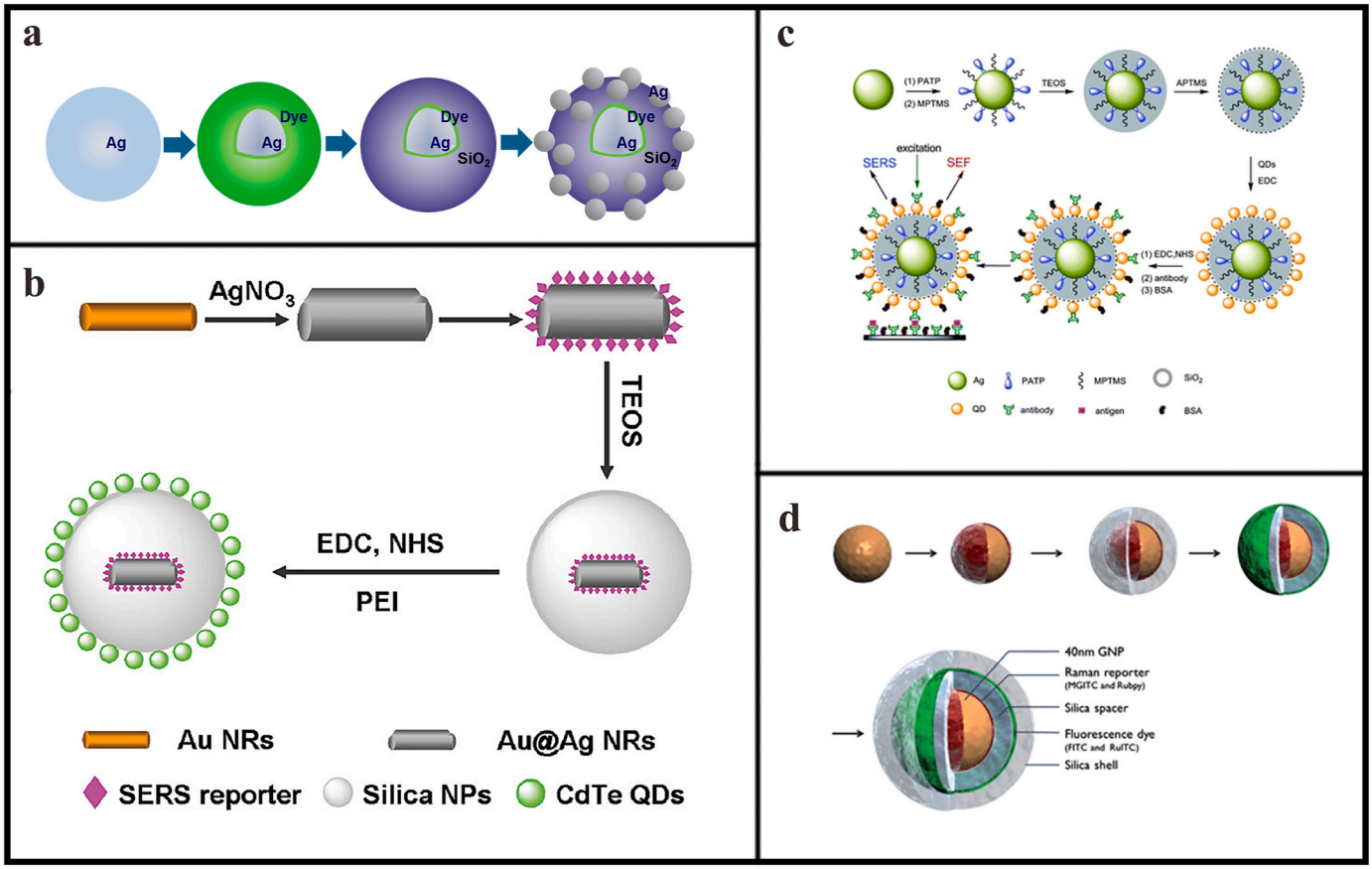

Fig. 8. (a) Schematic diagram of SERS Ag@SiO_2 synthesised by Ag satellite composite NPs. Reproduced with permission [67]. Copyright 2017, American Chemical Society. (b) Preparation of OMQ NPs. Reproduced with permission [118]. Copyright 2012, American Chemical Society. (c) Schematic diagram of preparation of Ag@SiO_2 SERS label nanocomposite modified by CdS quantum dots. Reproduced with permission [11]. Copyright 2013, The Royal Society of Chemistry. (d) Schematic diagram of preparation process of dual-mode SERS fluorescence imaging probe SiO_2 coated Au NPs. Reproduced with permission [119]. Copyright 2020, The Royal Society of Chemistry.

double-stranded co-expression markers on cancer cells (Fig. 8d) [119]. Combined with the advantages of fluorescence and SERS, these dual-mode nanostructures can be used as powerful probes for novel biomedical imaging.

3.2.2. SERS-SEF sensors based on other shell structure substrate

When fluorophores are situated at an optimal distance from the substrate surface (exceeding 50 Å), their emission intensity increases, thereby triggering the SEF effect. This effect is notably pronounced when the distance ranges from 70 to 100 Å. Provided that the distance to the surface remains relatively close, it is feasible to capture a composite spectrum of SERS and SEF. This dual-spectrum approach offers a comprehensive insight into the vibrational and electronic characteristics of molecules anchored on metal NPs. To maintain an optimal separation between the fluorophore and metal, the metal surface needs to be modified using appropriate spacers. In the beginning, a common approach was to cover NPs with spacers such as fatty acids or proteins. Accordingly, Lajos et al. studied the ionisation, aggregation and adsorption of the anti-tumour drug hypericin (Hyp) on the metal surface by using SERS and SEF technology [120], and they verified that the aggregation-self-spacing effect would occur between the ionisation state of Hyp and the surface of Ag NPs at different pHs, resulting in changes in the SERS–SEF spectrum. Osorio-Roman et al. observed the SERS and SEF effects of Rhodamine B (Rh B) molecules coated with Ag NPs with D-glucose as an organic coating, indicating the distance dependence of SERS and SEF on the coated Ag nano-structures [121]. In addition, polymer coatings have been reported as isolation layers to enable dual-mode SERS and SEF detection of metal NPs. Using poly-vinylpyrrolidone (PVP) as a polymer coating of Au nano-star particles, Tatar et al. tested the colour groups of Nile Blue A (NB) and Rhodamine 800 (Rh800) molecules under the influence of visible light (633 nm) and near-infrared (785 nm) laser excitation [122]. The effectiveness of

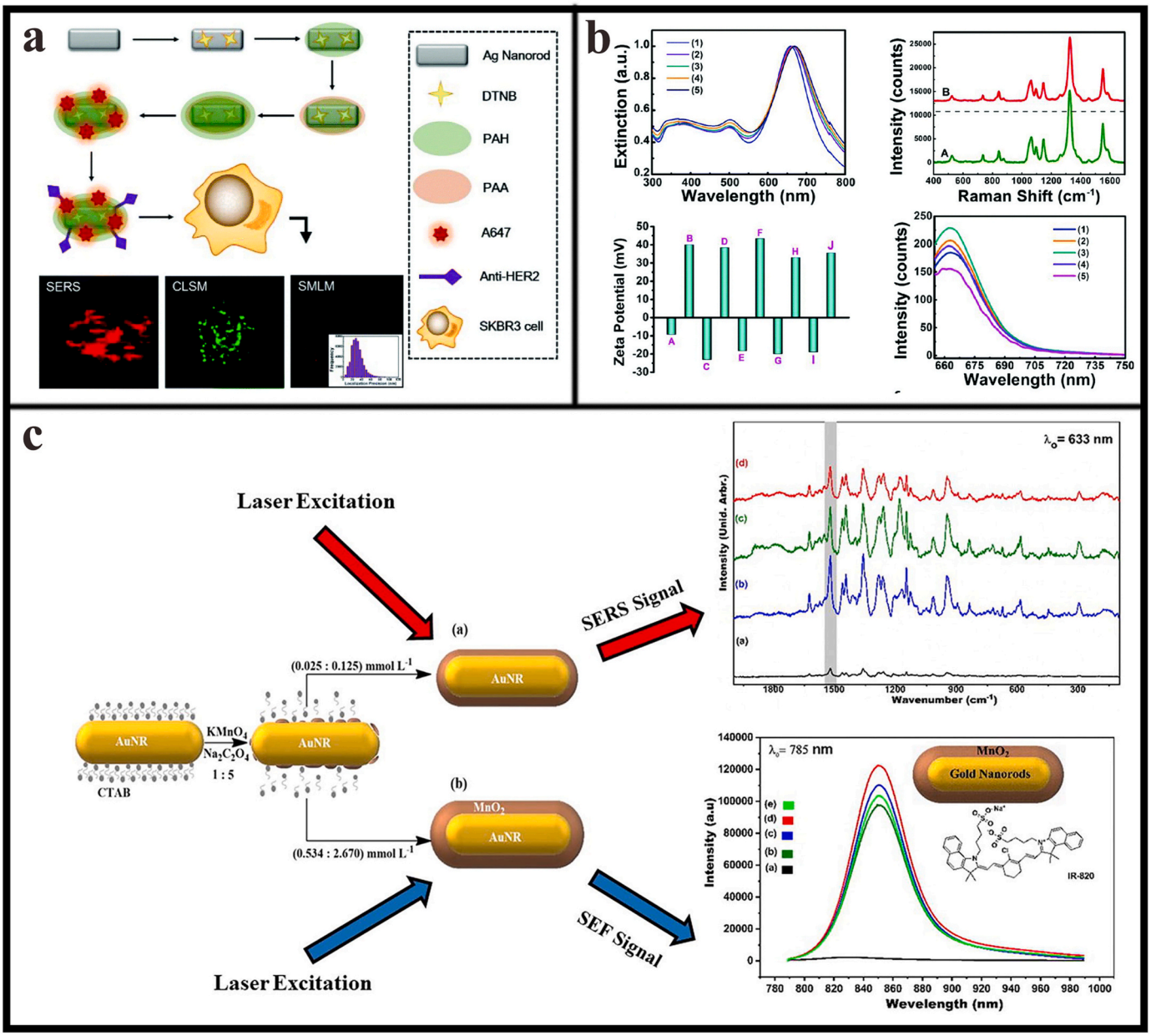

Fig. 9. (a) Schematic diagram of the preparation process of SERS SEF and superresolution three-mode nanoprobes; (b) Extinction spectrum, SERS spectrum, Zeta point site and SEF spectrum of the three-mode probe. Reproduced with permission [12]. Copyright 2020, The Royal Society of Chemistry. (c) Preparation of ultra-thin layer of manganese dioxide at Au NR@MnO_2 and its SERS and SEF spectroscopic evaluation. Reproduced with permission [86]. Copyright 2022, The Elsevier.

plasmonic membranes as dual-mode SEF and SERS substrates was proved. Zong et al. used Ag NRs as a kernel to attach Raman reporter molecules directly to the surface of Ag NRs to generate SERS signals (Fig. 9a and b) [12]. PEs were then coated as an isolation layer on Ag NRs, and the fluorophore was then connected to the PE layer as a nano-scale metal structure to achieve SERS and SEF effects. By virtue of the optimal structure, triple mode imaging of a breast cancer cell line (SKBR3) was achieved. Nicolas et al. fabricated alginate polymer–stabilised Ag NPs (AgALG) as a substrate and encased them in calcium alginate hydro-gel beads [123]. Alginate α-L-glutamyl uric acid (G) monomers bind to di-valent metals, such as Ca^{2+}, via carboxyl and hydroxyl groups to form cross-linked hydro-gels. In addition, negatively charged porous structures containing AgALG can interact with charged dyes via electro-static forces, resulting in SERS effects or SEF effects as spacers due to the short distance of AgALG from the dye.

Of the oxides used as shells, silica is undoubtedly the most studied, but it suffers the limitation of being sensitive to the high pH environment of dissolved SiO_2 shells. Therefore, a variety of oxides, such as aluminium oxide, manganese oxide and other metal oxide shells, have been used to replace SiO_2 [112,124]. Studies have recognised the MnO_x oxide layer for its ideal property of maintaining a uniform and dense shell at high pHs [124]. Accordingly, MnO_2 is highly stable in a strong alkaline medium; therefore, it is an interesting research direction to cover plasmonic NPs with MnO_2 and broaden the application field of SERS and SEF. Marques et al. prepared a MnO_2 ultra-thin layer covered with Au NRs (Au NR@MnO_2) with different thicknesses [86], and they characterised and evaluated the material obtained as an SERS and SEF substrate (Fig. 9c). The study showed that the fewer was the number of layers, the more significant was the EF in the SERS effect, while the opposite was true in the case of the SEF effect. This seemingly opposite behaviour of both plasmonic effects seemed to be attributable to the distance dependence of the EM field generated in Au NRs. In addition, the SERS–SEF two -mode substrate with a core–shell structure seemed to have a better anti-interference ability, which could overcome the influence of various extreme environmental factors, such as extreme pH, high pressure or high temperature, and obtain more valuable information.

Compared with that of noble metal substrates, the preparation cost of core–shell structured substrates is moderate because an insulating material (such as silica or alumina) needs to be coated on the surface of noble metal NPs, which increases the preparation steps and material costs. This structure has high stability, and the shell can effectively protect noble metal NPs in the core from oxidation or aggregation, as well as reduce the interference from environmental factors. The preparation process of the core–shell structure is relatively controllable, and good reproducibility can be achieved by precisely controlling the thickness and uniformity of the shell. The following points make this structure suitable for a variety of detection scenarios: 1) its detection sensitivity is high; 2) the enhancement effects of SERS and SEF can be balanced by optimising the shell thickness to avoid fluorescence quenching; 3) the SERS EF can reach 105 and the SEF EF 10^2.

3.3. SERS-SEF sensors based on non-noble metal substrate

While Au and Ag remain the predominant choices for SERS applications within the visible spectrum, Raman enhancement has also been noted on certain dielectric materials [125]. Unfortunately, almost all conventional semiconductors exhibit relatively low EF and millimole limit of detection (LOD), which fall short of the requirements for highly sensitive immunoassays [126]. Among the various approaches that have been developed in recent years, a new three-dimensional (3D) light-capture strategy has garnered attention [127]. Research has shown that the multiple reflections and scattering of electromagnetic waves within 3D nanostructures can elongate the optical path, enhance the interaction and charge transfer (CT) between photons and the semiconductor materials, and consequently result in a substantial boost in SERS performance [128–131]. Transition metal disulphides (TMDs) have received considerable attention because of their unique optical properties and flexible-manufacturing properties [132,133]. As luminescent emitters with large transition dipole moments, TMDs can also be combined with nano-cavities for plasmonic–exciton interactions when excitons and plasmon resonances are spectrometrically matched. This results in a massive fluorescence enhancement in the weakly coupled state via double resonance in the plasmonic mode [134,135]. Zhang et al. used this simultaneous SERS and SEF technique in monolayer $MoSe_2$-coupled plasmonic nanocavors (Fig. 10a) [87]. After optimising the spatial overlap and spectral overlap of excitons and plasmon resonances, the EFs of SERS and SEF exceed 10^7 and 6000, respectively, on the same nano-cube. Here, the gap provided by $MoSe_2$ and Al_2O_3 is the key to obtaining high EFs for both SERS and SEF.

Investigations of light–matter interactions to boost EM fields near optical nano-antennas remains a vibrant and intriguing research domain. Beyond the familiar electric-dipole resonance, dielectric nano-antennas can amplify the near field through more intricate EM configurations [137,138]. Meanwhile, plasmonic nanoantennas have been widely used in the fields of surface-enhanced Raman scattering [139,140], fluorescence emission [141,142], and plasmonic-induced chemistry [143]. A properly designed dielectric material allows for the probe to be positioned arbitrarily close to the antenna surface without suffering photo-bleaching, thermal dissociation [144], or reduced photon emission efficiency. Therefore, placing the probe near the all-dielectric antenna helps to improve the excitation enhancement required for surface-enhanced spectroscopy, while the risk of losing photons to the lossy channel is negligible [88]. Based on this, Cambiasso et al. prepared silicon nanodimers and coated them with a single layer of beta-carotene to detect surface-enhanced Raman scattering and fluorescence emission of the same probe [88]. The SERS factor and SEF factor for C–C bond stretching of a polyene chain are 1720 ± 300 and 470 ± 90, respectively (Fig. 10b). It is worth noting that in SERS, metal substrates typically provide stronger electric field enhancement than dielectrics due to the significant local field enhancement from plasmonic resonance. In contrast, SEF enhancement primarily relies on excitation enhancement (proportional to the square of the local electric field) and radiative efficiency (quantum yield). The low-loss nature of dielectric materials, such as silicon, leads to higher radiative efficiency for fluorescence emission, which can compensate for the weaker electric field enhancement compared to metals. Therefore, by optimising the geometry of the nanoantennas, the distance between the molecules and the antenna, and the excitation wavelength, significant enhancement in both SERS and SEF can be achieved, with comparable enhancement factors. Romano et al. proposed a fully dielectric meta-surface made of nano-structured transparent silicon nitride that supported a bound state in the continuum (BIC) (Fig. 10c) [89], achieving a simultaneous enhancement of fluorescence emission and far-field intensity of Raman scattering of molecules dispersed on these metasurface by a factor of 10^3. Aligning LSPR with the BIC field has been demonstrated to amplify traditional SERS signals by more than an order of magnitude. These findings hold significant potential for applications in enhanced sensing, Raman imaging and non-linear processes. Wells et al. demonstrated that coating the surface of silicon nano-wires (NWs) with a layer of zinc phthalocyanine with a thickness of <30 atomic molecules could generate a significant Raman spectrum with an EF better than two orders of magnitude [136]. The cylindrical and elliptical silicon nano-columns were labelled with different fluorophores and their SEF capability was evaluated (Fig. 10d). EFs derived upon analysing the fluorescence microscope images obtained showed that the silicon nano-column structure could provide comparable or even stronger enhancement than the plasmonic SEF structure, without the limitations associated with a metal-based substrate, such as fluorescence quenching and insufficient probe volume.

Graphene and carbon nitride materials have also been confirmed to possess both SERS and enhanced fluorescence properties. The extensive

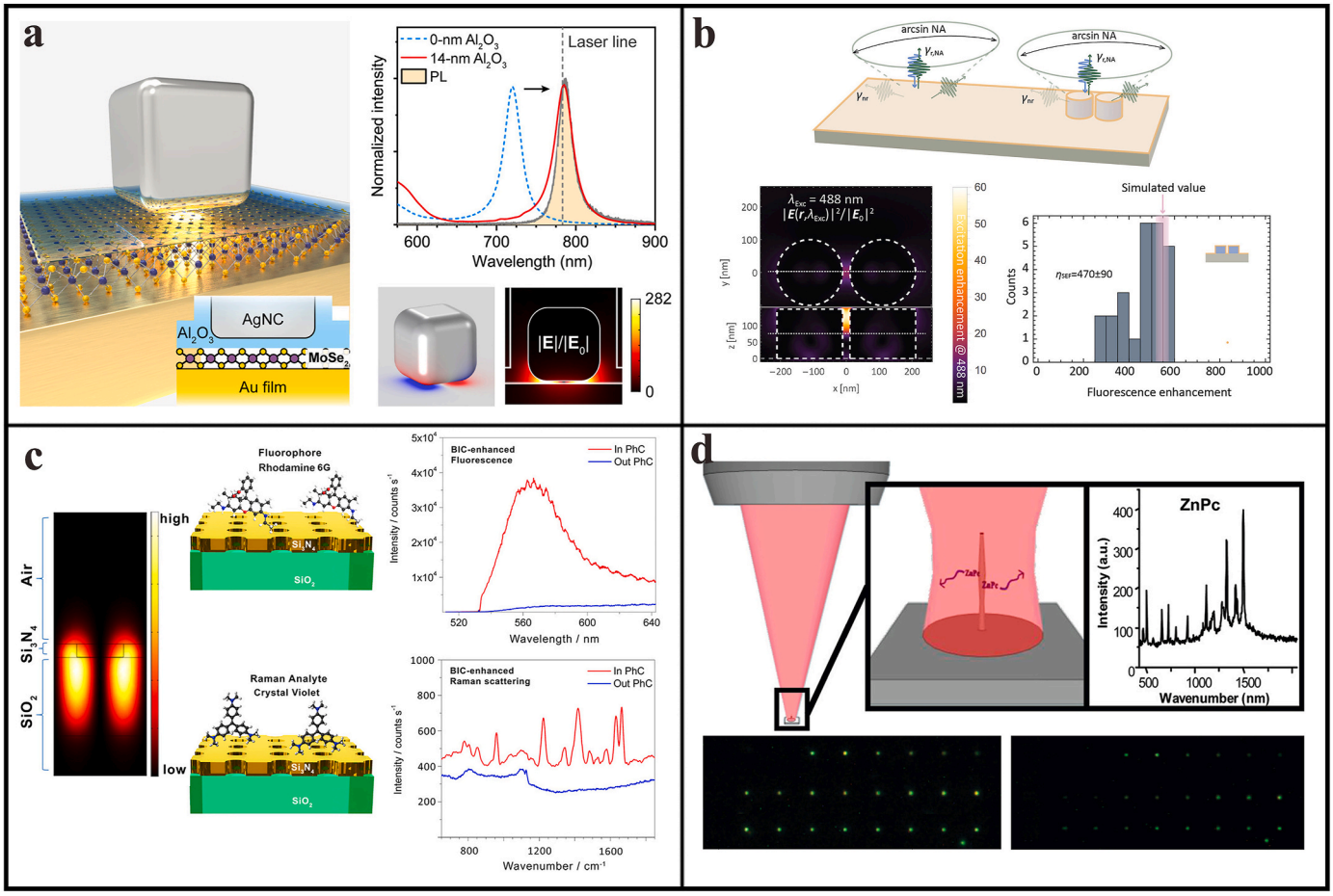

Fig. 10. (a) Three-dimensional diagram of $MoSe_2$-NCOM system, simulated scattering spectra of $MoSe_2$-NCOM, surface charge and electric field distribution at 785 nm. Reproduced with permission [87]. Copyright 2018, American Chemical Society. (b) The scheme for accurately modeling the fluorescence emission characteristics of the emitter on the substrate and antenna surface, the total excitation enhancement, the fluorescence rate enhancement histogram measured by experiment and the predicted value by theory are presented. Reproduced with permission [88]. Copyright 2018, American Chemical Society. (c) (left) Numerical simulation showing the electric field, (top) schematic layout of R6G on the sample surface and fluorescence emission spectrum. (below) Diagram of CV across the sample surface and Raman scattering spectrum. Reproduced with permission [89]. Copyright 2018, American Chemical Society. (d) Silicon nanocolumn detection schematic and fluorescence image. Reproduced with permission [136]. Copyright 2012, American Chemical Society. (For interpretation of the references to colour in this figure legend, the reader is referred to the Web version of this article.)

potential applications of graphene and its derivatives in enhancing fluorescence and Raman scattering, especially in the field of bio-medical detection and imaging, have been demonstrated [145]. For instance, Yang et al. fabricated a graphene-oxide-based SERS substrate by controlling the degree of reduction of graphene oxide (GO), and this substrate was then used to detect specific bio-markers of human neural stem cells [146]. Weng et al. combined graphene with carbon dots to create a fluorescent sensor for detecting vitamin B12, exhibiting high sensitivity and selectivity [147]. Pandit et al. explored through experiments and theoretical calculations the influence of GO on the fluorescence behaviour of fluorescent molecules (such as Oxazine-170 [OXO]) in various solvents, systematically studying the application of GO in enhancing fluorescence [148]. Their study demonstrated the complex role of GO in fluorescence enhancement and prototropism, emphasising the effect of GO on the behaviour of fluorescent molecules in different solvents and provided new insights for the application of GO in fluorescent sensing and imaging. Meanwhile, carbon nitride has also been reported to exhibit similar properties. Wang et al. introduced a recyclable, SERS-based immuno-assay for the tumour marker CA125, mediated by 1T-2H mixed-phase magnetic molybdenum di-sulphide (Fe_3O_4@MoS_2) probes and 2D graphitic carbon nitride (g-C_3N_4) nano-sheets [149]. In this study, Fe_3O_4@MoS_2 composites and g-C_3N_4 nano-sheets were rationally developed and combined to achieve recyclable SERS detection of CA125. The Fe_3O_4 core facilitated the reliable stacking of MoS_2 nano-flakes into a flower-like shape with fully exposed active surfaces. Particularly, the presence of the 1T phase enabled SERS activity comparable with that of noble metals because of the highly efficient CT process induced by high electron density. Moreover, bulk g-C_3N_4 was converted into 2D nano-sheets via acid etching, and the large surface area of these nano-sheets, rich in active electrons and functional groups, triggered an EF of 7.8×10^6. An LOD of 4.96×10^{-4} IU/mL was achieved for CA125 in a recyclable process based on a typical sandwich immuno-structure. Finally, this immuno-sensor was employed to analyse clinical samples, indicating its considerable potential in the early recognition and monitoring of cancer. Chen et al. reported a fluorescence enhancement phenomenon based on polymeric carbon nitride nano-sheets (PCN NSs) for bio-sensing applications [150]. It was observed that the fluorescence of tetramethylrhodamine (TMR)-labelled single-stranded DNA (ssDNA) was not quenched but enhanced upon adsorption on PCN NSs. This fluorescence enhancement was related to the guanine (G) bases near TMR. In the presence of PCN NSs, the photo-induced electron transfer quenching effect between TMR and G bases was shielded by the steric hindrance effect, resulting in the fluorescence enhancement of TMR-labelled ssDNA on PCN NSs. Based on this fluorescence enhancement effect and the change in the affinity of PCN NSs for ssDNA probes upon hybridisation with complementary

ssDNA, a versatile, ratiometric bio-sensing platform was demonstrated for the high-sensitivity fluorescence detection of ssDNA and microRNA. However, research on dual-mode SERS–SEF substrates of these two materials is still limited and can be an important focus area for future researchers.

The substrates of these non-precious metals (TMD, Si, etc.) exhibit a good dual-mode SERS–SEF function; moreover, the preparation cost of non-noble metal substrates (such as those of transition metal sulphides and silicon.) is low because these materials are inexpensive and some preparation methods (such as chemical vapour deposition and sol–gel method) are relatively simple. However, non-noble metal materials have relatively poor chemical stability and are susceptible to environmental factors (such as pH and temperature), but their stability can be improved by optimisation of structural design (such as forming core–shell structures). The preparation process is sensitive to experimental conditions, and there may be some differences between batches of products; however, the reproducibility can be improved by optimising the process. SERS and SEF EFs obtained using non-noble metal materials are relatively lower than those obtained using noble metals, but their detection sensitivity can be significantly improved via structural design optimisation (such as forming nano-arrays and core–shell structures), with SERS EFs reaching 10^4 and SEF EFs reaching 10^3, which are suitable for routine detection. Therefore, core–shell noble metal substrates are still our first choice, of which SERS and SEF substrates based on SHINs or like-SHINs (such as metal oxide shells [124] or molecularly imprinted shell [41]) exhibit better shell-thickness adjustability, which is more conducive to the design of dual-mode SERS–SEF substrates with a high EF.

4. Application of SERS-SEF dual-mode substrates

Dual-mode SERS–SEF substrates have a wide application prospect in the detection of environmental pollutants and food, bio-medical analysis and drug analysis among other applications [151]. This part mainly focuses on the practical application of the dual-mode SERS–SEF detection platform and covers the application status of a small part of a typical SERS–fluorescence dual-mode-detection platform and a single-mode-detection platform in extreme environments.

4.1. Environmental pollutants and food analysis

The detection of dyes, pigments and other such substances is of considerable significance in environmental protection, human health security and quality control among other fields. Through detection, its pollution in water bodies, soil and atmosphere can be detected and controlled in a timely manner, reducing the potential harm to the ecosystem and human health [7,152]. Cao et al. successfully achieved ultra-low concentration detection of the toxic dye CV by preparing Ag nano-islands on wheat leaves as substrates and using the SERS and SEF techniques, with an LOD as low as 10^{-10} M [153]. Tang et al. formed Ag nano-structured gratings with triangular cross-sections by sputtering Ag films on pre-stretched PDMS substrates and releasing stress [34]. These structures exhibited extremely high SEF and SERS activities because of the EM field enhancement effect at their sharp peaks and could be used to detect crystal CV and R6G molecules at concentrations as low as 10^{-14} M. This method was effective and low-cost for creating pleated periodic singular patterns for various applications. Meanwhile, dyes such as R6G and Rh B are also frequently used as probe molecules to verify the performance research of dual-mode SERS–SEF substrates. In addition, the dual-mode SERS–SEF technology is used to detect pesticide residues, heavy metal ions, pathogenic bacteria, etc. in the environment and organisms. Huang et al. fabricated a 3D random cross-over wire stacking structure platform based on Ag NWs [154]. This structure forms abundant hot spots through multi-layer stacking of Ag NWs, significantly enhancing the local electromagnetic field, thereby achieving a dual enhancement effect of SERS and SEF for four pesticides (including fluoxonil which is difficult to detect by traditional SERS methods). It can achieve a detection limit of 5 μM–0.05 μM within a tiny analysis volume of 20 μL. In addition, the SERS-SEF dual-modal detection platform is also used for the detection of Hg^{2+} in adulterated milk samples, the assessment of mercury levels in chicken tissues and eggs with a high-mercury diet, and the different interactions between pathogenic Escherichia coli strains and AuNPs (especially the biochemical changes at the cellular level) [155–157].

4.2. Biomedical and drug detection

SYBR Green I is a fluorescent dye widely employed in polymerase chain reactions (PCRs) and bio-fluorescence imaging. Guo et al., through SERS and SEF technology, utilised the enhancement effect of Ag NPs to improve the detection sensitivity for SYBR Green I [10]. The SERS EF measured in the experiment was 3.2×10^3, indicating that SERS could be used for the quantitative detection of SYBR Green I. Meanwhile, Ag NPs increased the fluorescence signal intensity of SYBR Green I by approximately two times. This technique was able to improve the sensitivity for SYBR Green I in PCR, thereby improving the resolution of biological imaging, and could be generalised to high-sensitivity detection of other materials as well. Han et al. prepared an active substrate via Ag colloid staining, and they used tetramethylrhodamine isothiocyanate (TRITC) and Atto610 as Raman and fluorescent probes to detect interactions between human immunoglobulin G (IgG) and TRITC-anti-human IgG and streptavidin and ATto610-biotin [97]. The method used SERRS and SEF effects of Ag NPs to significantly improve the sensitivity and light stability of protein detection, and it demonstrated the potential of high sensitivity, high-throughput, chip-based determination of protein function. Zhang et al. investigated the application of QD-modified Ag@SiO_2 nano-structures in SERS and SEF. Antibody-modified, QD-modified Ag@SiO_2 nano-composites were used to achieve efficient antigen immuno-assays through SERS and SEF [11]. This study demonstrated the potential to simultaneously achieve SERS and SEF in biological detection and imaging through the rational design and control of multi-functional nano-structures.

Diabetes is a severe health problem, and the detection of blood sugar levels is crucial for the early diagnosis of diabetes. Traditional blood glucose detection methods suffer problems of inconvenience and low sensitivity; although the SERS technology offers high sensitivity and selectivity, its practical application is limited by the complex manufacturing process and low reproducibility. Lu et al. designed a two-mode fluorescence –SERS method for blood glucose detection with respect to diabetes screening. Using 4-mercaptophenylboric acid and 4-cyanophenylboric acid as sugar recognition molecules, different concentrations of glucose solutions were detected through SERS [73]. Real human blood samples were used to confirm the detection capability of the dual-mode platform, and the results were consistent with clinical reports. This means that the dual-mode SERS–SEF platform had high sensitivity and good reproducibility, was suitable for large-scale diabetes screening and had cost-effective and practical application potential. In addition, the testing of anti-tumour drugs not only helps ensure the safety and effectiveness of treatment but also provides important support for drug research and development and clinical trials. The behaviour and mechanism of action of drugs can be deeply studied by integrating modern detection technologies (such as SERS and SEF), providing a scientific basis for the development of new drugs and the optimisation of treatment plans. Through the SERS and SEF techniques, Lajos et al. systematically investigated the behaviour of the anti-tumour drug Hyp on the surface of Ag NPs and the mechanism of the enhancement of the drug's fluorescence [120]. The research results demonstrated that SERS could provide information regarding the structure and adsorption state of Hyp molecules on the surface of Ag NPs. SEF could enhance the fluorescence signal of Hyp, and the enhancement mechanism was verified through fluorescence lifetime measurements. Thereafter, Sevilla et al. used the anti-tumour drug

emodin as a research object; they combined the SERS and SEF techniques to study the behaviour of emodin on the surface of Ag NPs and the mechanism of the enhancement of emodin's fluorescence under different pH conditions [158]. Studies have shown that SERS and SEF techniques can provide molecular behavior information of emodin under different physiological conditions (such as aggregation state, adsorption state, etc.), which is of great significance for understanding the metabolic process and mechanism of action of drugs in the body. Tatar et al. conducted SERS and SEF detections of Nile Blue A (NB) and Rhodamine 800 (Rh800) using self-assembled PVP-Au nanofilm (GNSts) films [122]. The results show that these molecules can be detected based on SERS fingerprint bands even under fluorescence resonance excitation conditions, even in the presence of strong fluorescence. To demonstrate the extended application of substrates in the detection of biorelated molecules, the authors tested the detection efficiency of GNStsPVP films for metanephrine (a metabolite currently used in the biochemical diagnosis of neuroendocrine tumors). Experiments demonstrated that GNStPVP films could detect metanephrine at a concentration level similar to that of catecholamine metabolites. Although the practical application of this technology in the detection of neuro-transmitters is still in its infancy, this research demonstrated its potential application value.

4.3. Extreme environments

Acidic environments (such as those associated with gastric juice and acidic mine wastewater) are harmful to many organisms, but certain micro-organisms (such as *Helicobacter pylori*) can survive in these environments. The development of probes capable of detecting bio-molecules in acidic environments is of considerable significance for studying the metabolic and adaptation mechanisms of these micro-organisms. Ag2S QDs synthesised by Zhao et al. using the seed-mediated method could detect bio-molecules in extremely acidic environments and serve as pH sensors, exhibiting good linear relationships and reversibility [159]. A coumarin-based fluorescent probe, namely CMM, prepared by Li et al. could detect hydrazine and pH changes in extremely acidic environments and exhibited good stability and selectivity [160]. A novel Th^{4+} fluorescent probe, BH-TPE (N1', N2'-bis((3-hydroxytetrastyrene-2yl)methylene)malonohydrazide), was designed and synthesised [161]. his probe delivered remarkable performance in the detection of Th^{4+} under extremely acidic conditions. It not only exhibited high selectivity and sensitivity but also enabled live cell imaging and real water sample detection, providing new methods and tools for environmental monitoring and bio-medical research on Th^{4+}.

In addition, extreme environments also include the deep sea, the polar regions and extraterrestrial stars, etc. Especially in the deep-sea extreme environment (cold seeps and hydrothermal vents), there are rich biological resources and unique chemical processes. Surface-enhanced Raman scattering (SERS) and fluorescence techniques have gradually become important analytical tools in extreme environments due to their high sensitivity, non-destructibility and rapid detection capabilities. Wang et al. were the first to design a deep-sea in situ SERS probe and propose a protection strategy for SERS substrates [162]. Subsequently, they successfully employed it to an internal biological community of cold-seep vents in the South China Sea, obtaining for the first time the Raman signals of acetyl-CoA, carotene and various amino acids in the deep sea in situ [163]. Subsequently, Wang et al. further designed a variety of SERS substrates (metal sponge structure and flexible fabric base) suitable for in situ deep-sea work, and they proposed a deep-sea drop-type probe system [164]. These research works provided new technical means for further expanding the application fields of SERS and facilitating the detection of trace/ultra-trace key substances in deep-sea extreme environments. Hu et al. developed a micro-fluidic fluorescence sensing device based on paper and cloth; the device utilised Au NPs and Rh B molecules fixed on the cloth substrate to detect L-cysteine [165]. The practical application ability of the device was verified by analysing deep-sea, cold-seep water samples from the South China Sea, with the recovery rate being 98.07 %–102.62 %. Du et al. developed an in situ detection instrument based on ultra-violet laser (266 nm)–induced fluorescence for the detection of three natural aromatic amino acids in seawater: tryptophan, tyrosine and phenylalanine. Their research offered a practical method for detecting deep-sea aromatic amino acids, which not only offered enhanced detection efficiency but also provided a new approach for the understanding of marine organic matter and the nitrogen cycle [166]. In addition, Eshelman et al. presented a 'deep ultra-violet' fluorescence spectrometer called WATSON (Wireline Analysis Tool for the Subsurface Observation of Northern ice sheets) [167]. WATSON is a compact instrument used for ice core analysis and mapping the spatial distribution of organic matter and micro-organisms. It can detect organic matter and micro-organisms in ice and can be used for the exploration of the earth's glaciers and ice caps, as well as the surfaces associated with celestial bodies such as those of Mars' poles, Europa (a moon of Jupiter) and Enceladus (a moon of Saturn). Through non-destructive testing and highly sensitive fluorescence spectroscopy technology, WATSON can detect trace amounts of organic matter and micro-organisms in complex ice environments, which holds a significant scientific value for studying life activities in ice layers and searching for extra-terrestrial life. Sunuwar et al. studied the low-temperature fluorescence excitation and emission spectra of chloro-benzene, benzoic acid, phthalic acid, mellitic acid and benzene in water ice solution, with a temperature range of 78 K–273 K [168]. These spectral data helped explain the origin of chloro-benzene on Mars and provided a reference for the design of fluorescence experiments in future Mars missions. Tang et al. proposed a spectral sensing technique based on non-fluorescent SERS for detecting organic compounds at sub-ppm levels in Mars-like soil [169]. This technology combines 1064-nm laser excitation and nano-structure enhancement, significantly improving the detection sensitivity for extremely low concentrations of organic substances. By enhancement in detection sensitivity and reduction in fluorescence interference, this technology can effectively detect organic bio-markers that may exist in Martian soil, thereby providing a powerful evidence for whether life exists on Mars or ever existed. Mareč kova et al. studied the photo-synthetic performance of the Antarctic lichen *Dermatocarpon polyphyllizum* at various temperatures [170]. Through chlorophyll fluorescence analysis, it was observed that low temperature significantly affected the function of optical system II. The key temperature was −12 °C, at which time the main process of photo-synthesis was completely inhibited. By determining key temperature points and sensitive fluorescence parameters, this study provided a scientific basis for the protection and research of polar ecosystems in future. Moreover, these findings contributed to predicting and assessing the effect of climate change on polar ecosystems.

In conclusion, the study of extreme environments, especially those associated with the deep sea and exoplanets, is of extra-ordinary significance. It holds an immeasurable value in many aspects, such as exploring the mysteries of nature, expanding the boundaries of human cognition and facilitating the development of science and technology. However, in the face of the complexity and particularity of extreme environments, a single technical means often seems inadequate and experiences difficulty in achieving comprehensive, in-depth and precise detection. Meanwhile, the content of relevant organic molecules in extreme environments is usually extremely low, which further increases the difficulty of detection. Hence, establishing a dual-mode SERS–SEF (or multi-mode) detection platform is undoubtedly a highly forward-looking and strategic measure. With its unique advantages and powerful functions, this platform may provide solid, reliable, highly innovative technical support for achieving all-round, full-scale detection in extreme environments in future, thereby helping humanity take more solid and powerful steps in the exploration of extreme environments.

5. Conclusions and perspectives

Dual-mode SERS–SEF tags offer the combined advantages of intuitive and fast fluorescence imaging and the multiplexing capability of SERS, and they have considerable potential in bio-detection and bio-imaging. In recent years, considerable efforts have been made in the manufacturing of dual-mode SERS–SEF substrates, and the structural morphology, preparation technology and potential applications of these substrates have been studied in detail. As described herein, some mechanisms and properties of these dual-mode substrates have been proposed, which have considerably facilitated the development of dual-mode SERS–SEF detection. However, in near future, we speculate that the SHIN structure of noble metal NPs may be one of the most promising technologies and the mainstream choice for dual-mode SERS–SEF substrates. Most importantly, the distance between fluorescence and SERS probe molecules can be easily controlled by regulating the shell thickness, and the design of the distance should consider the signal strength and the characteristics of the system. In addition, a number of issues need to be addressed to achieve the practical applications of these promising technologies:

1. The enhancement mechanism of the SERS-SEF dual-modal substrate is still unclear and needs to be determined. Although several mechanisms have been proposed to explain SERS or SEF phenomena, including the combined effect of LSPR on SERS and SEF. But so far, none of these mechanisms can explain all the SERS-SEF phenomena. Multi-physics coupling simulation can be introduced to simulate the dynamic process of nanostructures under photoexcitation, such as considering the photothermal effect, charge transfer and other multi-physics coupling factors. This helps to understand how SPR affects both SERS and SEF signals under real detection conditions.
2. Although some non-metallic plasmonic substrates have been developed and proved to have both SERS and SEF enhanced properties. However, their application scenarios are very limited, and their application potential and application prospect need to be further developed. Applying it to more extreme environmental fields is an effective means to broaden its application scenarios.
3. Because SERS and SEF have different requirements for reporting the distance between molecules and the substrate, Raman needs to be close to the substrate to obtain a higher enhancement factor, but it will lead to fluorescence quenching. How to effectively solve the defect that the enhancement effect of dual-function platform is not as good as that of single-function platform, while obtaining the best enhancement performance of SERS and SEF? Reasonable control of the distance between molecules and nanostructures is one of the effective solutions.
4. Improving the stability, repeatability and accuracy of the detection performance of SERS-SEF dual-modal substrate is a major challenge for product commercialization and practical application. For example, standardizing preparation processes, testing conditions, and data processing.
5. How to use various enhanced spectral techniques to probe the boundaries of human cognition, such as deep space and deep sea and other extreme fields. For example, reasonably design the protection device of the substrate, or improve the anti-interference ability of the substrate to cope with the complex conditions of the extreme environment.
6. Comprehensive evaluation of waste substrate treatment measures and environmental effects. For some metal substrates, chemical reagents can be used for dissolution recovery. For example, for Ag substrates, an oxidizing acid such as nitric acid can be used for dissolution. Nitric acid will chemically react with Ag to form soluble salts such as silver nitrate.
7. This dual-modal platform is in environmental monitoring, food safety, material science and so on. The application in such fields is still in its infancy. We should conduct a more in-depth study of its coupling mechanism to enhance the application potential of the SERS-SEF dual-modal platform.
8. One disadvantage of the intended approach is the requirements for more equipment, that can hamper miniaturization. Therefore, designing corresponding multispectral detection devices is also a development trend in the future.
9. SERS-SEF substrates that preconcentrate/detect (combined with nanomaterials) can be very competitive. This integrated SERS-SEF substrate can offer higher sensitivity, lower detection limits, and a simpler operating procedure, which endows it with broad application prospects in the fields of biomedical detection, environmental monitoring, and food safety.

We expect the dual-mode SERS–SEF analysis technology to become a powerful tool that would not be merely limited to the detection of biomolecules, DNA and living cells and in vivo biological imaging, but also would be successfully applied for analysing more extreme environments (for example, deep sea, polar and other extreme environments) by virtue of the protective effect of the inert shell.

CRediT authorship contribution statement

Siyu Wang: Writing – original draft. **Bowei Li:** Writing – review & editing, Methodology, Investigation, Conceptualization. **Jiawen Xiang:** Writing – original draft, Investigation, Formal analysis, Conceptualization. **Lianfu Li:** Supervision, Investigation. **Shichuan Xi:** Investigation, Formal analysis. **Ruhao Pan:** Resources. **Zhendong Luan:** Supervision, Formal analysis. **Lingxin Chen:** Writing – review & editing, Supervision, Conceptualization. **Xin Zhang:** Writing – review & editing, Supervision, Funding acquisition.

Declaration of competing interest

The authors declare that they have no known competing financial interests or personal relationships that could have appeared to influence the work reported in this paper.

Acknowledgments

This research was supported by the following grants: the National Natural Science Foundation of China (42327805, 42221005, 42376188, 22376216); the Natural Science Foundation of Shandong Province (ZR2024QD137, ZR2024MB066); the China Postdoctoral Science Foundation (2024M761249); Key project of Ocean Research Center, Chinese Academy of Sciences (COMS2020J03, COMS2019J01); National Natural Science Foundation of China (12204527); Qingdao science and technology benefit the people demonstration project (23-2-8-cspz-5-nsh), and the Synergetic Extreme Condition User Facility (2023-SECUF-PT-000701).

Data availability

Data will be made available on request.

References

[1] S. Abalde-Cela, S. Carregal-Romero, J.P. Coelho, A. Guerrero-Martínez, Recent progress on colloidal metal nanoparticles as signal enhancers in nanosensing, Adv. Colloid Interfac. 233 (2016) 255–270, https://doi.org/10.1016/j.cis.2015.05.002.

[2] H. Li, S.A. Haruna, W. Sheng, Q. Bei, W. Ahmad, M. Zareef, et al., SERS-Activated platforms for chemical contaminants in food: probes, encoding methods, and detection, TrAC, Trends Anal. Chem. 169 (2023) 117365, https://doi.org/10.1016/j.trac.2023.117365.

[3] W.-I.K. Chio, H. Xie, Y. Zhang, Y. Lan, T.-C. Lee, SERS biosensors based on cucurbituril-mediated nanoaggregates for wastewater-based epidemiology, TrAC, Trends Anal. Chem. 146 (2022) 116485, https://doi.org/10.1016/j.trac.2021.116485.

[4] Y. Jeong, Y.-M. Kook, K. Lee, W.-G. Koh, Metal enhanced fluorescence (MEF) for biosensors: general approaches and a review of recent developments, Biosens. Bioelectron. 111 (2018) 102–116, https://doi.org/10.1016/j.bios.2018.04.007.
[5] M.A. Badshah, N.Y. Koh, A.W. Zia, N. Abbas, Z. Zahra, M.W. Saleem, Recent developments in plasmonic nanostructures for metal enhanced fluorescence-based biosensing, Nanomaterials 10 (2020) 1749, https://doi.org/10.3390/nano10091749.
[6] P.-P. Fang, X. Lu, H. Liu, Y. Tong, Applications of shell-isolated nanoparticles in surface-enhanced raman spectroscopy and fluorescence, TrAC, Trends Anal. Chem. 66 (2015) 103–117, https://doi.org/10.1016/j.trac.2014.11.015.
[7] S. Balbinot, A.M. Srivastav, J. Vidic, I. Abdulhalim, M. Manzano, Plasmonic biosensors for food control, Trends Food Sci. Technol. 111 (2021) 128–140, https://doi.org/10.1016/j.tifs.2021.02.057.
[8] I. Abdulhalim, Plasmonic sensing using metallic nano-sculptured thin films, Small 10 (2014) 3499–3514, https://doi.org/10.1002/smll.201303181.
[9] L. Lu, S. Guan, Y. Guan, M. Hong, Dual-modal fluorescence-SERS detection of blood glucose engineered by hierarchical laser-induced micro/nano structures for diabetes screening, Adv. Mater. Interfac. 9 (2022) 2102532, https://doi.org/10.1002/admi.202102532.
[10] W. Guo, J. Wu, C. Wang, T. Zhang, T. Chen, Application of silver nanoparticles in the detection of SYBR green I by surface enhanced Raman and surface-enhanced fluorescence, J Nanopart. Res. 20 (2018) 122, https://doi.org/10.1007/s11051-018-4228-0.
[11] X. Zhang, X. Kong, Z. Lv, S. Zhou, X. Du, Bifunctional quantum dot-decorated Ag@SiO_2 nanostructures for simultaneous immunoassays of surface-enhanced Raman scattering (SERS) and surface-enhanced fluorescence (SEF), J. Mater. Chem. B 1 (2013) 2198–2204, https://doi.org/10.1039/C3TB20069H.
[12] S. Zong, H. Tang, K. Yang, H. Wang, Z. Wang, Y. Cui, SERS-fluorescence-superresolution triple-mode nanoprobe based on surface enhanced Raman scattering and surface enhanced fluorescence, J. Mater. Chem. B 8 (2020) 8459–8466, https://doi.org/10.1039/D0TB01211D.
[13] F. Li, S. Wang, H. Yin, Y. Chen, Y. Zhou, J. Huang, et al., Photoelectrochemical biosensor for DNA formylation detection in genomic DNA of maize seedlings based on black TiO_2-enhanced photoactivity of MoS_2/WS_2 heterojunction, ACS Sens. 5 (2020) 1092–1101, https://doi.org/10.1021/acssensors.0c00036.
[14] F. Li, Y. Zhou, H. Yin, S. Ai, Recent advances on signal amplification strategies in photoelectrochemical sensing of microRNAs, Biosens. Bioelectron. 166 (2020) 112476, https://doi.org/10.1016/j.bios.2020.112476.
[15] X. Bi, D.M. Czajkowsky, Z. Shao, J. Ye, Digital colloid-enhanced Raman spectroscopy by single-molecule counting, Nature 628 (2024) 771–775, https://doi.org/10.1038/s41586-024-07218-1.
[16] S. Zong, Z. Wang, R. Zhang, C. Wang, S. Xu, Y. Cui, A multiplex and straightforward aqueous phase immunoassay protocol through the combination of SERS-fluorescence dual mode nanoprobes and magnetic nanobeads, Biosens. Bioelectron. 41 (2013) 745–751, https://doi.org/10.1016/j.bios.2012.09.057.
[17] H.-Y. Hsieh, T.-W. Huang, J.-L. Xiao, C.-S. Yang, C.-C. Chang, C.-C. Chu, et al., Fabrication and modification of dual-faced nano-mushrooms for tri-functional cell theranostics: sers/fluorescence signaling, protein targeting, and drug delivery, J. Mater. Chem. 22 (2012) 20918–20928, https://doi.org/10.1039/C2JM32967K.
[18] Y. Zhang, J. Qian, D. Wang, Y. Wang, S. He, Multifunctional gold nanorods with ultrahigh stability and tunability for in vivo fluorescence imaging, SERS detection, and photodynamic therapy, Angew. Chem. Int. Ed. 52 (2013) 1148–1151, https://doi.org/10.1002/anie.201207909.
[19] Y. Wang, L. Chen, P. Liu, Biocompatible Triplex Ag@SiO_2@mTiO_2 core–shell nanoparticles for simultaneous fluorescence-SERS bimodal imaging and drug delivery, Chem. Eur J. 18 (2012) 5935–5943, https://doi.org/10.1002/chem.201103571.
[20] Q. Yang, Y. Wu, J. Chen, M. Lu, X. Wang, Z. Zhang, et al., Plasmonic nanomaterial-enhanced fluorescence and Raman sensors: multifunctional platforms and applications, Coord. Chem. Rev. 507 (2024) 215768, https://doi.org/10.1016/j.ccr.2024.215768.
[21] A. Merlen, F. Lagugné-Labarthet, E. Harté, Surface-enhanced Raman and fluorescence spectroscopy of dye molecules deposited on nanostructured gold surfaces, J. Phys. Chem. C 114 (2010) 12878–12884, https://doi.org/10.1021/jp101576h.
[22] P. Johansson, H. Xu, M. Käll, Surface-enhanced Raman scattering and fluorescence near metal nanoparticles, Phys. Rev. B 72 (2005) 035427, https://doi.org/10.1103/PhysRevB.72.035427.
[23] A.M. Gabudean, M. Focsan, S. Astilean, Gold nanorods performing as dual-modal nanoprobes via metal-enhanced fluorescence (MEF) and surface-enhanced Raman scattering (SERS), J. Phys. Chem. C 116 (2012) 12240–12249, https://doi.org/10.1021/jp211954m.
[24] Y. Yang, J.M. Callahan, T.-H. Kim, A.S. Brown, H.O. Everitt, Ultraviolet nanoplasmonics: a demonstration of surface-enhanced Raman spectroscopy, fluorescence, and photodegradation using gallium nanoparticles, Nano Lett. 13 (2013) 2837–2841, https://doi.org/10.1021/nl401145j.
[25] R.F. Aroca, G.Y. Teo, H. Mohan, A.R. Guerrero, P. Albella, F. Moreno, Plasmon-Enhanced fluorescence and spectral modification in SHINEF, J. Phys. Chem. C 115 (2011) 20419–20424, https://doi.org/10.1021/jp205997u.
[26] A.R. Guerrero, R.F. Aroca, Surface-enhanced fluorescence with shell-isolated nanoparticles (SHINEF), Angew. Chem. Int. Ed. 50 (2011) 665–668, https://doi.org/10.1002/anie.201004806.
[27] G. Sabatté, R. Keir, M. Lawlor, M. Black, D. Graham, W.E. Smith, Comparison of surface-enhanced resonance Raman scattering and fluorescence for detection of a labeled antibody, Anal. Chem. 80 (2008) 2351–2356, https://doi.org/10.1021/ac071343j.
[28] J. Yang, Z. Wang, S. Zong, H. Chen, R. Zhang, Y. Cui, Dual-mode tracking of tumor-cell-specific drug delivery using fluorescence and label-free SERS techniques, Biosens. Bioelectron. 51 (2014) 82–89, https://doi.org/10.1016/j.bios.2013.07.034.
[29] J.M. McMahon, S. Li, L.K. Ausman, G.C. Schatz, Modeling the effect of small gaps in surface-enhanced Raman spectroscopy, J. Phys. Chem. C 116 (2012) 1627–1637, https://doi.org/10.1021/jp207661y.
[30] H. Wei, H. Xu, Hot spots in different metal nanostructures for plasmon-enhanced Raman spectroscopy, Nanoscale 5 (2013) 10794–10805, https://doi.org/10.1039/C3NR02924G.
[31] M.J. Banholzer, J.E. Millstone, L. Qin, C.A. Mirkin, Rationally designed nanostructures for surface-enhanced Raman spectroscopy, Chem. Soc. Rev. 37 (2008) 885–897, https://doi.org/10.1039/B710915F.
[32] Y. Ying, Z. Tang, Y. Liu, Material design, development, and trend for surface-enhanced Raman scattering substrates, Nanoscale 15 (2023) 10860–10881, https://doi.org/10.1039/D3NR01456H.
[33] S.-C. Luo, K. Sivashanmugan, J.-D. Liao, C.-K. Yao, H.-C. Peng, Nanofabricated SERS-active substrates for single-molecule to virus detection in vitro: a review, Biosens. Bioelectron. 61 (2014) 232–240, https://doi.org/10.1016/j.bios.2014.05.013.
[34] J. Tang, H. Guo, M. Chen, J. Yang, D. Tsoukalas, B. Zhang, et al., Wrinkled Ag nanostructured gratings towards single molecule detection by ultrahigh surface Raman scattering enhancement, Sensor. Actuat. B-Chem. 218 (2015) 145–151, https://doi.org/10.1016/j.snb.2015.04.008.
[35] P.A. Mosier-Boss, Review of SERS substrates for chemical sensing, Nanomaterials 7 (2017) 142, https://doi.org/10.3390/nano7060142.
[36] J. Jin, Z. Guo, D. Fan, B. Zhao, Spotting the driving forces for SERS of two-dimensional nanomaterials, Mater. Horiz. 10 (2023) 1087–1104, https://doi.org/10.1039/D2MH01241C.
[37] M.F. Cardinal, E. Vander Ende, R.A. Hackler, M.O. McAnally, P.C. Stair, G. C. Schatz, et al., Expanding applications of SERS through versatile nanomaterials engineering, Chem. Soc. Rev. 46 (2017) 3886–3903, https://doi.org/10.1039/C7CS00207F.
[38] A. Sultangaziyev, R. Bukasov, Review: applications of surface-enhanced fluorescence (SEF) spectroscopy in bio-detection and biosensing, Sens. Biosens. Res. 30 (2020) 100382, https://doi.org/10.1016/j.sbsr.2020.100382.
[39] J. Chen, L. Guo, B. Qiu, Z. Lin, T. Wang, Application of ordered nanoparticle self-assemblies in surface-enhanced spectroscopy, Mater. Chem. Front. 2 (2018) 835–860, https://doi.org/10.1039/C7QM00557A.
[40] Y.-J. Zhang, P.M. Radjenovic, X.-S. Zhou, H. Zhang, J.-L. Yao, J.-F. Li, Plasmonic core–shell nanomaterials and their applications in spectroscopies, Adv. Mater. 33 (2021) 2005900, https://doi.org/10.1002/adma.202005900.
[41] Y. Yang, X. Liu, S. Meng, S. Mao, W. Tao, Z. Li, Molecularly imprinted polymers-isolated AuNP-enhanced CdTe QD fluorescence sensor for selective and sensitive oxytetracycline detection in real water samples, J. Hazard Mater. 458 (2023) 131941, https://doi.org/10.1016/j.jhazmat.2023.131941.
[42] L.K. Ausman, G.C. Schatz, On the importance of incorporating dipole reradiation in the modeling of surface enhanced Raman scattering from spheres, J. Chem. Phys. 131 (2009), https://doi.org/10.1063/1.3211969.
[43] K.-i. Yoshida, T. Itoh, H. Tamaru, V. Biju, M. Ishikawa, Y. Ozaki, Quantitative evaluation of electromagnetic enhancement in surface-enhanced resonance Raman scattering from plasmonic properties and morphologies of individual Ag nanostructures, Phys. Rev. B 81 (2010) 115406, https://doi.org/10.1103/PhysRevB.81.115406.
[44] X. Yu, X. Tang, J.Y. Dong, Y. Deng, M. Saito, Z. Gao, et al., Defect-Engineered coordination compound nanoparticles based on prussian blue analogues for surface-enhanced raman spectroscopy, ACS Nano 18 (2024) 30987–31001, https://doi.org/10.1021/acsnano.4c06972.
[45] S.J. Lee, Z. Guan, H. Xu, M. Moskovits, Surface-enhanced Raman spectroscopy and nanogeometry: the plasmonic origin of SERS, J. Phys. Chem. C 111 (2007) 17985–17988, https://doi.org/10.1021/jp077422g.
[46] L. Salomon, G. Bassou, H. Aourag, J.P. Dufour, F. de Fornel, F. Carcenac, et al., Local excitation of surface plasmon polaritons at discontinuities of a metal film: theoretical analysis and optical near-field measurements, Phys. Rev. B 65 (2002) 125409, https://doi.org/10.1103/PhysRevB.65.125409.
[47] Y. Zhao, M. Sun, W. Ma, H. Kuang, C. Xu, Biological molecules-governed plasmonic nanoparticle dimers with tailored optical behaviors, J. Phys. Chem. Lett. 8 (2017) 5633–5642, https://doi.org/10.1021/acs.jpclett.7b01781.
[48] S.-Y. Ding, E.-M. You, Z.-Q. Tian, M. Moskovits, Electromagnetic theories of surface-enhanced Raman spectroscopy, Chem. Soc. Rev. 46 (2017) 4042–4076, https://doi.org/10.1039/C7CS00238F.
[49] K.-i. Yoshida, T. Itoh, V. Biju, M. Ishikawa, Y. Ozaki, Experimental evaluation of the twofold electromagnetic enhancement theory of surface-enhanced resonance Raman scattering, Phys. Rev. B 79 (2009) 085419, https://doi.org/10.1103/PhysRevB.79.085419.
[50] T. Itoh, K.-i. Yoshida, H. Tamaru, V. Biju, M. Ishikawa, Experimental demonstration of the electromagnetic mechanism underlying surface enhanced Raman scattering using single nanoparticle spectroscopy, J. Photochem. Photobiol., A 219 (2011) 167–179, https://doi.org/10.1016/j.jphotochem.2011.03.001.
[51] J.B. Jackson, N.J. Halas, Surface-enhanced Raman scattering on tunable plasmonic nanoparticle substrates, Proc. Natl. Acad. Sci. 101 (2004) 17930–17935, https://doi.org/10.1073/pnas.0408319102.

[52] T. Itoh, M. Procházka, Z.-C. Dong, W. Ji, Y.S. Yamamoto, Y. Zhang, et al., Toward a new era of SERS and TERS at the nanometer scale: from fundamentals to innovative applications, Chem. Rev. 123 (2023) 1552–1634, https://doi.org/10.1021/acs.chemrev.2c00316.
[53] A.R.L. Marshall, J. Stokes, F.N. Viscomi, J.E. Proctor, J. Gierschner, J.-S. G. Bouillard, et al., Determining molecular orientation via single molecule SERS in a plasmonic nano-gap, Nanoscale 9 (2017) 17415–17421, https://doi.org/10.1039/C7NR05107G.
[54] L. Zhang, H. Liu, L. Chen, P. Guan, B. Chen, T. Fujita, et al., Large-scale growth of sharp gold nano-cones for single-molecule SERS detection, RSC Adv. 6 (2016) 2882–2887, https://doi.org/10.1039/C5RA22321K.
[55] M. Kerker, D.S. Wang, H. Chew, Surface enhanced Raman scattering (SERS) by molecules adsorbed at spherical particles, Appl. Opt. 19 (1980) 3373–3388, https://doi.org/10.1364/AO.19.003373.
[56] S. Habouti, C.-H. Solterbeck, M. Es-Souni, Synthesis of silver nano-fir-twigs and application to single molecules detection, J. Mater. Chem. 20 (2010) 5215–5219, https://doi.org/10.1039/C0JM00564A.
[57] C.D. Geddes, Metal-enhanced fluorescence, Phys. Chem. Chem. Phys. 15 (2013), https://doi.org/10.1039/C3CP90129G, 19537-19537.
[58] C. Geddes, J. Lakowicz, Metal-enhanced fluorescence, J. Fluoresc. 12 (2002) 121–129, https://doi.org/10.1023/A:1016875709579.
[59] K.H. Drexhage, Influence of a dielectric interface on fluorescence decay time, J. Lumin. 1–2 (1970) 693–701, https://doi.org/10.1016/0022-2313(70)90082-7.
[60] K.H. Drexhage, M. Fleck, Wide-angle interference and multipole nature of fluorescence and phosphorescence of organic dyes, Ber. Buns. phys. Chem. 72 (1968), https://doi.org/10.1002/bbpc.19680720262, 330-330.
[61] S.Z. Uddin, M.R. Tanvir, M.A. Talukder, A proposal and a theoretical analysis of an enhanced surface plasmon coupled emission structure for single molecule detection, J. Appl. Phys. 119 (2016) 204701, https://doi.org/10.1063/1.4952576.
[62] C.-Y. Li, Z.-W. Yang, J.-C. Dong, T. Ganguly, J.-F. Li, Plasmon-enhanced spectroscopies with shell-isolated nanoparticles, Small 13 (2017) 1601598, https://doi.org/10.1002/smll.201601598.
[63] A.R. Guerrero, Y. Zhang, R.F. Aroca, Experimental confirmation of local field enhancement determining far-field measurements with shell-isolated silver nanoparticles, Small 8 (2012) 2964–2967, https://doi.org/10.1002/smll.201200750.
[64] Y. Zhou, P. Zhang, Simultaneous SERS and surface-enhanced fluorescence from dye-embedded metal core–shell nanoparticles, Phys. Chem. Chem. Phys. 16 (2014) 8791–8794, https://doi.org/10.1039/C4CP01199F.
[65] Y. Kitahama, M. Funaoka, Y. Ozaki, Plasmon-enhanced optical tweezers for single molecules on and near a colloidal silver nanoaggregate, J. Phys. Chem. C 123 (2019) 18001–18006, https://doi.org/10.1021/acs.jpcc.9b05626.
[66] Y. Kitahama, Y. Nishiyama, Y. Ozaki, Blinking surface-enhanced Raman scattering and fluorescence from a single silver nanoaggregate simultaneously analyzed by bi-color intensity ratios and a truncated power law, J. Phys. Chem. C 122 (2018) 22106–22113, https://doi.org/10.1021/acs.jpcc.8b06920.
[67] S. Chang, S.L. Eichmann, T.-Y.S. Huang, W. Yun, W. Wang, Controlled design and fabrication of SERS–SEF multifunctional nanoparticles for nanoprobe applications: morphology-dependent SERS phenomena, J. Phys. Chem. C 121 (2017) 8070–8076, https://doi.org/10.1021/acs.jpcc.7b00688.
[68] T. Itoh, Y.S. Yamamoto, H. Tamaru, V. Biju, N. Murase, Y. Ozaki, Excitation laser energy dependence of surface-enhanced fluorescence showing plasmon-induced ultrafast electronic dynamics in dye molecules, Phys. Rev. B 87 (2013) 235408, https://doi.org/10.1103/PhysRevB.87.235408.
[69] H. Cao, Z. Shang, H. Cao, Y. Hou, Y. Yang, Z. Sun, et al., An efficient and low-cost surface-enhanced fluorescence substrate for trace detection of melamine in milk samples, Optik 268 (2022) 169856, https://doi.org/10.1016/j.ijleo.2022.169856.
[70] A. Loiseau, V. Asila, G. Boitel-Aullen, M. Lam, M. Salmain, S. Boujday, Silver-based plasmonic nanoparticles for and their use in biosensing, Biosensors 9 (2019) 78, https://doi.org/10.3390/bios9020078.
[71] V. Amendola, M. Meneghetti, What controls the composition and the structure of nanomaterials generated by laser ablation in liquid solution? Phys. Chem. Chem. Phys. 15 (2013) 3027–3046, https://doi.org/10.1039/C2CP42895D.
[72] R. Bardhan, N.K. Grady, J.R. Cole, A. Joshi, N.J. Halas, Fluorescence enhancement by Au nanostructures: nanoshells and nanorods, ACS Nano 3 (2009) 744–752, https://doi.org/10.1021/nn900001q.
[73] L. Lu, J. Zhang, L. Jiao, Y. Guan, Large-scale fabrication of nanostructure on bio-metallic substrate for surface enhanced Raman and fluorescence scattering, Nanomaterials 9 (2019) 916, https://doi.org/10.3390/nano9070916.
[74] J. Tang, H.F. Wen, P.L. Chai, J. Liu, Y.B. Shi, C.Y. Xue, Study of surface Raman and fluorescence enhancement of RhB molecules adsorbed on Au nanoparticles, J. Nano Res. 20 (2012) 33–41. https://doi.org/10.4028/www.scientific.net/JNanoR.20.33.
[75] P. Chai, P. Chai, J. Liu, J. Liu, J. Tang, J. Tang, et al., Base Effects on Fluorescence and Surface-Enhanced Raman Scattering of Crystal Violet Adsorbed on Au Nanoparticles Surface, J. Nanosci. Nanotechnol. 13 (2013) 1011–1016, https://doi.org/10.1166/jnn.2013.6103.
[76] C.J.L. Constantino, R.F. Aroca, C.R. Mendonça, S.V. Mello, D.T. Balogh, O. N. Oliveira, Surface enhanced fluorescence and Raman imaging of Langmuir-Blodgett azopolymer films, Spectrochim. Acta 57 (2001) 281–289, https://doi.org/10.1016/S1386-1425(00)00373-5.
[77] R.F. Aroca, C.J.L. Constantino, J. Duff, Surface-enhanced Raman scattering and imaging of Langmuir—Blodgett monolayers of Bis(Phenethylimido)perylene on silver island films, Appl. Spectrosc. 54 (2000) 1120–1125, https://doi.org/10.1366/0003702001950913.
[78] T. Itoh, Y.S. Yamamoto, Reproduction of surface-enhanced resonant Raman scattering and fluorescence spectra of a strong coupling system composed of a single silver nanoparticle dimer and a few dye molecules, J. Chem. Phys. 149 (2018) 244701, https://doi.org/10.1063/1.5061816.
[79] G.P. Acuna, F.M. Möller, P. Holzmeister, S. Beater, B. Lalkens, P. Tinnefeld, Fluorescence enhancement at docking sites of DNA-directed self-assembled nanoantennas, Science 338 (2012) 506–510, https://doi.org/10.1126/science.1228638.
[80] M.-Z. Zhao, X. Wang, Y.-K. Xing, S.-K. Ren, N. Teng, J. Wang, et al., DNA origami-templated assembly of plasmonic nanostructures with enhanced Raman scattering, Nucl. Sci. Tech. 29 (2017) 6, https://doi.org/10.1007/s41365-017-0347-z.
[81] J. Dong, S. Qu, H. Zheng, Z. Zhang, J. Li, Y. Huo, et al., Simultaneous SEF and SERRS from silver fractal-like nanostructure, Sensor. Actuat. B-Chem. 191 (2014) 595–599, https://doi.org/10.1016/j.snb.2013.09.088.
[82] G.Q. Wallace, M. Tabatabaei, R. Hou, M.J. Coady, P.R. Norton, T.S. Simpson, et al., Superimposed arrays of nanoprisms for multispectral molecular plasmonics, ACS Photonics 3 (2016) 1723–1732, https://doi.org/10.1021/acsphotonics.6b00388.
[83] P.J. Tarcha, J. Desaja-Gonzalez, S. Rodriguez-Llorente, R. Aroca, Surface-enhanced fluorescence on SiO_2-coated silver island films, Appl. Spectrosc. 53 (1999) 43–48, https://doi.org/10.1366/0003702991945443.
[84] H. Pei, Y. Wei, D. Guo, B. Wang, F. Wang, Numerical investigations of Au@SiO_2 dimers for shell-isolated nanoparticles enhanced Raman scattering and fluorescence, Optik 181 (2019) 978–983, https://doi.org/10.1016/j.ijleo.2018.12.146.
[85] Y. Wei, L. Li, D. Sun, Y. Zhu, G. Tian, The effect of silica shell on the surface enhanced Raman scattering and fluorescence with Ag nanoparticles: a three-dimensional finite element method investigation, Opt. Commun. 427 (2018) 426–432, https://doi.org/10.1016/j.optcom.2018.06.086.
[86] F.C. Marques, G.C. Azevedo, C.A. Senna, B.S. Archanjo, C.C. Corrêa, R.C. Matos, et al., Structural characterization and plasmonic properties of manganese oxide-coated gold nanorods, Spectrochim. Acta 272 (2022) 120988, https://doi.org/10.1016/j.saa.2022.120988.
[87] Y. Zhang, W. Chen, T. Fu, J. Sun, D. Zhang, Y. Li, et al., Simultaneous surface-enhanced resonant Raman and fluorescence spectroscopy of monolayer $MoSe_2$: determination of ultrafast decay rates in nanometer dimension, Nano Lett. 19 (2019) 6284–6291, https://doi.org/10.1021/acs.nanolett.9b02425.
[88] J. Cambiasso, M. König, E. Cortés, S. Schlücker, S.A. Maier, Surface-enhanced spectroscopies of a molecular monolayer in an all-dielectric nanoantenna, ACS Photonics 5 (2018) 1546–1557, https://doi.org/10.1021/acsphotonics.7b01604.
[89] S. Romano, G. Zito, S. Managò, G. Calafiore, E. Penzo, S. Cabrini, et al., Surface-enhanced Raman and fluorescence spectroscopy with an all-dielectric metasurface, J. Phys. Chem. C 122 (2018) 19738–19745, https://doi.org/10.1021/acs.jpcc.8b03190.
[90] M. Prochazka, Bioanalytical SERS applications, Biolog. Med. Phys. Biomed. Eng. (2016) 61–91, https://doi.org/10.1007/978-3-319-23992-7_4.
[91] M.K. Hossain, Y. Kitahama, G.G. Huang, T. Kaneko, Y. Ozaki, SPR and SERS characteristics of gold nanoaggregates with different morphologies, Appl. Phys. B 93 (2008) 165–170, https://doi.org/10.1007/s00340-008-3193-1.
[92] A. Roguska, A. Kudelski, M. Pisarek, M. Opara, M. Janik-Czachor, Surface-enhanced Raman scattering (SERS) activity of Ag, Au and Cu nanoclusters on TiO_2-nanotubes/Ti substrate, Appl. Surf. Sci. 257 (2011) 8182–8189, https://doi.org/10.1016/j.apsusc.2010.12.048.
[93] J. Yue, Z. Liu, X. Cai, X. Ding, S. Chen, K. Tao, et al., Bull serum albumin coated au@agnanorods as SERS probes for ultrasensitive osteosarcoma cell detection, Talanta 150 (2016) 503–509, https://doi.org/10.1016/j.talanta.2015.12.065.
[94] Y. Ling, Y. Zhuo, L. Huang, D. Mao, Using Ag-embedded TiO_2 nanotubes array as recyclable SERS substrate, Appl. Surf. Sci. 388 (2016) 169–173, https://doi.org/10.1016/j.apsusc.2016.01.257.
[95] C.J.L. Constantino, R.F. Aroca, Surface-enhanced resonance Raman scattering imaging of Langmuir–Blodgett monolayers of bis(benzimidazo)perylene on silver island films, J. Raman Spectrosc. 31 (2000) 887–890, https://doi.org/10.1002/1097-4555(200010)31:10<887::AID-JRS603>3.0.CO;2-V.
[96] M.L. Roldán, G. Corrado, O. Francioso, S. Sanchez-Cortes, Interaction of soil humic acids with herbicide paraquat analyzed by surface-enhanced Raman scattering and fluorescence spectroscopy on silver plasmonic nanoparticles, Anal. Chim. Acta 699 (2011) 87–95, https://doi.org/10.1016/j.aca.2011.05.001.
[97] X.X. Han, Y. Kitahama, Y. Tanaka, J. Guo, W.Q. Xu, B. Zhao, et al., Simplified protocol for detection of protein−ligand interactions via surface-enhanced resonance raman scattering and surface-enhanced fluorescence, Anal. Chem. 80 (2008) 6567–6572, https://doi.org/10.1021/ac800642g.
[98] T. Itoh, M. Iga, H. Tamaru, K.-i. Yoshida, V. Biju, M. Ishikawa, Quantitative evaluation of blinking in surface enhanced resonance Raman scattering and fluorescence by electromagnetic mechanism, J. Chem. Phys. 136 (2012) 24703, https://doi.org/10.1063/1.3675567.
[99] J. Ou, H. Tan, X. Chen, Z. Chen, DNA-assisted assembly of gold nanostructures and their induced optical properties, Nanomaterials 8 (2018) 994, https://doi.org/10.3390/nano8120994.
[100] D. Signe, L. Frances, M. Antony, M. Mark, P. Robert, H.R. James, Effect of matrix on Raman scattering and luminescence in 2D gold nanorod arrays, Proc. SPIE 9126 (2014) 91262I, https://doi.org/10.1117/12.2051913.
[101] A. Murphy, Y. Sonnefraud, A.V. Krasavin, P. Ginzburg, F. Morgan, J. McPhillips, et al., Fabrication and optical properties of large-scale arrays of gold nanocavities

based on rod-in-a-tube coaxials, Appl. Phys. Lett. 102 (2013) 103103, https://doi.org/10.1063/1.4794935.
[102] M.D. Doherty, A. Murphy, R.J. Pollard, P. Dawson, Surface-enhanced Raman scattering from metallic nanostructures: bridging the gap between the near-field and far-field responses, Phys. Rev. X 3 (2013) 011001, https://doi.org/10.1103/PhysRevX.3.011001.
[103] G.A. Wurtz, R. Pollard, W. Hendren, G.P. Wiederrecht, D.J. Gosztola, V. A. Podolskiy, et al., Designed ultrafast optical nonlinearity in a plasmonic nanorod metamaterial enhanced by nonlocality, Nat. Nanotechnol. 6 (2011) 107–111, https://doi.org/10.1038/nnano.2010.278.
[104] P.R. Evans, R. Kullock, W.R. Hendren, R. Atkinson, R.J. Pollard, L.M. Eng, Optical transmission properties and electric field distribution of interacting 2D silver nanorod arrays, Adv. Funct. Mater. 18 (2008) 1075–1079, https://doi.org/10.1002/adfm.200701289.
[105] E. Fort, S. Grésillon, Surface enhanced fluorescence, J. Phys. D Appl. Phys. 41 (2008) 013001, https://doi.org/10.1088/0022-3727/41/1/013001.
[106] W. Wei, F. Bai, H. Fan, Oriented gold nanorod arrays: Self-assembly and optoelectronic applications, Angew. Chem. Int. Ed. 58 (2019) 11956–11966, https://doi.org/10.1002/anie.201902620.
[107] S. Damm, F. Lordan, A. Murphy, M. McMillen, R. Pollard, J.H. Rice, Application of AAO matrix in aligned gold nanorod array substrates for surface-enhanced fluorescence and Raman scattering, Plasmonics 9 (2014) 1371–1376, https://doi.org/10.1007/s11468-014-9751-y.
[108] D. Signe, L. Frances, M. Antony, M. Mark, P. Robert, H.R. James, Control over plasmon enhanced Raman and fluorescence from quasi free-standing Au nanorod arrays, Proc. SPIE 9169 (2014) 91690T, https://doi.org/10.1117/12.2061677.
[109] M. Wang, X. Yan, G. Shi, Z. Shang, A. Zhang, W. Ma, Optical properties of Ag@cicada wing substrate deposited by Ag nanoparticles, Curr. Appl. Phys. 20 (2020) 1253–1262, https://doi.org/10.1016/j.cap.2020.08.013.
[110] C.-H. Zhang, J. Zhu, J.-J. Li, J.-W. Zhao, Focus and enlarge the enhancement region of local electric field by overlapping Ag triangular nanoplates, Eur. Phys. J. Appl. Phys. 73 (2016) 10501, https://doi.org/10.1051/epjap/2015150404.
[111] M.B. Newmai, M. Verma, P.S. Kumar, Monomer functionalized silica coated with Ag nanoparticles for enhanced SERS hotspots, Appl. Surf. Sci. 440 (2018) 133–143, https://doi.org/10.1016/j.apsusc.2018.01.007.
[112] J.F. Li, X.D. Tian, S.B. Li, J.R. Anema, Z.L. Yang, Y. Ding, et al., Surface analysis using shell-isolated nanoparticle-enhanced Raman spectroscopy, Nat. Protoc. 8 (2013) 52–65, https://doi.org/10.1038/nprot.2012.141.
[113] B.-Q. Zhang, S.-B. Li, Q. Xiao, J. Li, J.-J. Sun, Rapid synthesis and characterization of ultra-thin shell Au@SiO_2 nanorods with tunable SPR for shell-isolated nanoparticle-enhanced Raman spectroscopy (SHINERS), J. Raman Spectrosc. 44 (2013) 1120–1125, https://doi.org/10.1002/jrs.4336.
[114] X.-D. Tian, B.-J. Liu, J.-F. Li, Z.-L. Yang, B. Ren, Z.-Q. Tian, SHINERS and plasmonic properties of Au Core SiO_2 shell nanoparticles with optimal core size and shell thickness, J. Raman Spectrosc. 44 (2013) 994–998, https://doi.org/10.1002/jrs.4317.
[115] J.F. Li, Y.F. Huang, Y. Ding, Z.L. Yang, S.B. Li, X.S. Zhou, et al., Shell-isolated nanoparticle-enhanced Raman spectroscopy, Nature 464 (2010) 392–395, https://doi.org/10.1038/nature08907.
[116] J.R. Anema, J.-F. Li, Z.-L. Yang, B. Ren, Z.-Q. Tian, Shell-Isolated nanoparticle-enhanced raman spectroscopy: expanding the versatility of surface-enhanced raman scattering, Annu. Rev. Anal. Chem. 4 (2011) 129–150, https://doi.org/10.1146/annurev.anchem.111808.073632.
[117] X.-D. Lin, J.-F. Li, Y.-F. Huang, X.-D. Tian, V. Uzayisenga, S.-B. Li, et al., Shell-isolated nanoparticle-enhanced Raman spectroscopy: nanoparticle synthesis, characterization and applications in electrochemistry, J. Electroanal. Chem. 688 (2013) 5–11, https://doi.org/10.1016/j.jelechem.2012.07.017.
[118] Z. Wang, S. Zong, W. Li, C. Wang, S. Xu, H. Chen, et al., SERS-fluorescence joint spectral encoding using organic–metal–QD hybrid nanoparticles with a huge encoding capacity for high-throughput biodetection: putting theory into practice, J. Am. Chem. Soc. 134 (2012) 2993–3000, https://doi.org/10.1021/ja208154m.
[119] S. Lee, H. Chon, S.-Y. Yoon, E.K. Lee, S.-I. Chang, D.W. Lim, et al., Fabrication of SERS-fluorescence dual modal nanoprobes and application to multiplex cancer cell imaging, Nanoscale 4 (2012) 124–129, https://doi.org/10.1039/C1NR11243K.
[120] G. Lajos, D. Jancura, P. Miskovsky, J.V. García-Ramos, S. Sanchez-Cortes, Surface-enhanced fluorescence and Raman scattering study of antitumoral drug hypericin: an effect of aggregation and self-spacing depending on pH, J. Phys. Chem. C 112 (2008) 12974–12980, https://doi.org/10.1021/jp8034117.
[121] I.O. Osorio-Román, V. Ortega-Vásquez, V. Vargas C, R.F. Aroca, Surface-enhanced spectra on D-gluconic acid coated silver nanoparticles, Appl. Spectrosc. 65 (2011) 838–843, https://doi.org/10.1366/11-06279.
[122] A.-S. Tatar, S. Boca, A. Falamas, D. Cuibus, C. Farcău, Self-assembled PVP-gold nanostar films as plasmonic substrates for surface-enhanced spectroscopies: influence of the polymeric coating on the enhancement efficiency, Analyst 148 (2023) 3992–4001, https://doi.org/10.1039/D3AN00682D.
[123] M.F. Nicolas, J.H. Marin, G.T. Paganoto, R.F. Fernandes, M.L.A. Temperini, Surface-Enhanced Raman and Surface-enhanced fluorescence of charged dyes based on alginate silver nanoparticles and its calcium alginate hydrogel beads, Spectrochim. Acta 276 (2022) 121211, https://doi.org/10.1016/j.saa.2022.121211.
[124] H.B. Abdulrahman, K. Kołątaj, P. Lenczewski, J. Krajczewski, A. Kudelski, MnO_2-protected silver nanoparticles: new electromagnetic nanoresonators for Raman analysis of surfaces in basis environment, Appl. Surf. Sci. 388 (2016) 704–709, https://doi.org/10.1016/j.apsusc.2016.01.262.
[125] G. Wang, R. Yi, X. Zhai, R. Bian, Y. Gao, D. Cai, et al., A flexible SERS-active film for studying the effect of non-metallic nanostructures on Raman enhancement, Nanoscale 10 (2018) 16895–16901, https://doi.org/10.1039/C8NR04971H.
[126] M. Yilmaz, E. Babur, M. Ozdemir, R.L. Gieseking, Y. Dede, U. Tamer, et al., Nanostructured organic semiconductor films for molecular detection with surface-enhanced Raman spectroscopy, Nat. Mater. 16 (2017) 918–924, https://doi.org/10.1038/nmat4957.
[127] X. Zheng, W. Zhang, J. Zhang, L. Wang, Synthesis of yolk-shell Fe_3O_4@void@CeO_2 nanoparticles and their application in SERS, Appl. Surf. Sci. 541 (2021) 148422, https://doi.org/10.1016/j.apsusc.2020.148422.
[128] X. Wang, W. Shi, Z. Jin, W. Huang, J. Lin, G. Ma, et al., Remarkable SERS activity observed from amorphous ZnO nanocages, Angew. Chem. Int. Ed. 56 (2017) 9851–9855, https://doi.org/10.1002/anie.201705187.
[129] H. Qiu, M. Wang, L. Zhang, M. Cao, Y. Ji, S. Kou, et al., Wrinkled 2H-phase MoS_2 sheet decorated with graphene-microflowers for ultrasensitive molecular sensing by plasmon-free SERS enhancement, Sensor. Actuat. B-Chem. 320 (2020) 128445, https://doi.org/10.1016/j.snb.2020.128445.
[130] J. Ma, W. Dong, T. Xu, G. Wei, C. Gu, T. Jiang, A non-metallic SERS-based immunoassay founded by light-harvesting effect and strengthened chemical enhancement, Analyst 148 (2023) 1752–1763, https://doi.org/10.1039/D3AN00171G.
[131] W. Li, L. Xiong, N. Li, S. Pang, G. Xu, C. Yi, et al., Tunable 3D light trapping architectures based on self-assembled $SnSe_2$ nanoplate arrays for ultrasensitive SERS detection, J. Mater. Chem. C 7 (2019) 10179–10186, https://doi.org/10.1039/C9TC03715B.
[132] A. Splendiani, L. Sun, Y. Zhang, T. Li, J. Kim, C.-Y. Chim, et al., Emerging photoluminescence in monolayer MoS_2, Nano Lett. 10 (2010) 1271–1275, https://doi.org/10.1021/nl903868w.
[133] W. Chen, S. Zhang, M. Kang, W. Liu, Z. Ou, Y. Li, et al., Probing the limits of plasmonic enhancement using a two-dimensional atomic crystal probe, Light Sci. Appl. 7 (2018) 56, https://doi.org/10.1038/s41377-018-0056-3.
[134] G.M. Akselrod, T. Ming, C. Argyropoulos, T.B. Hoang, Y. Lin, X. Ling, et al., Leveraging nanocavity harmonics for control of optical processes in 2D semiconductors, Nano Lett. 15 (2015) 3578–3584, https://doi.org/10.1021/acs.nanolett.5b01062.
[135] Z. Wang, Z. Dong, Y. Gu, Y.-H. Chang, L. Zhang, L.-J. Li, et al., Giant photoluminescence enhancement in tungsten-diselenide–gold plasmonic hybrid structures, Nat. Commun. 7 (2016) 11283, https://doi.org/10.1038/ncomms11283.
[136] S.M. Wells, I.A. Merkulov, I.I. Kravchenko, N.V. Lavrik, M.J. Sepaniak, Silicon nanopillars for field-enhanced surface spectroscopy, ACS Nano 6 (2012) 2948–2959, https://doi.org/10.1021/nn204110z.
[137] G. Grinblat, Y. Li, M.P. Nielsen, R.F. Oulton, S.A. Maier, Enhanced third harmonic generation in single germanium nanodisks excited at the anapole mode, Nano Lett. 16 (2016) 4635–4640, https://doi.org/10.1021/acs.nanolett.6b01958.
[138] V. Rutckaia, F. Heyroth, A. Novikov, M. Shaleev, M. Petrov, J. Schilling, Quantum dot emission driven by mie resonances in silicon nanostructures, Nano Lett. 17 (2017) 6886–6892, https://doi.org/10.1021/acs.nanolett.7b03248.
[139] S. Schlücker, Surface-enhanced Raman spectroscopy: concepts and chemical applications, Angew. Chem. Int. Ed. 53 (2014) 4756–4795, https://doi.org/10.1002/anie.201205748.
[140] S. Simoncelli, E.-M. Roller, P. Urban, R. Schreiber, A.J. Turberfield, T. Liedl, et al., Quantitative single-molecule surface-enhanced Raman scattering by optothermal tuning of DNA origami-assembled plasmonic nanoantennas, ACS Nano 10 (2016) 9809–9815, https://doi.org/10.1021/acsnano.6b05276.
[141] O.L. Muskens, V. Giannini, J.A. Sánchez-Gil, J. Gómez Rivas, Strong enhancement of the radiative decay rate of emitters by single plasmonic nanoantennas, Nano Lett. 7 (2007) 2871–2875, https://doi.org/10.1021/nl0715847.
[142] M. Ringler, A. Schwemer, M. Wunderlich, A. Nichtl, K. Kürzinger, T.A. Klar, et al., Shaping emission spectra of fluorescent molecules with single plasmonic nanoresonators, Phys. Rev. Lett. 100 (2008) 203002, https://doi.org/10.1103/PhysRevLett.100.203002.
[143] W. Xie, S. Schlücker, Hot electron-induced reduction of small molecules on photorecycling metal surfaces, Nat. Commun. 6 (2015) 7570, https://doi.org/10.1038/ncomms8570.
[144] M. Caldarola, P. Albella, E. Cortés, M. Rahmani, T. Roschuk, G. Grinblat, et al., Non-plasmonic nanoantennas for surface enhanced spectroscopies with ultra-low heat conversion, Nat. Commun. 6 (2015) 7915, https://doi.org/10.1038/ncomms8915.
[145] S. Cortijo-Campos, R. Ramírez-Jiménez, A. de Andrés, Raman and fluorescence enhancement approaches in graphene-based platforms for optical sensing and imaging, Nanomaterials 11 (2021) 644, https://doi.org/10.3390/nano11030644.
[146] L. Yang, J.-H. Lee, C. Rathnam, Y. Hou, J.-W. Choi, K.-B. Lee, Dual-enhanced Raman scattering-based characterization of stem cell differentiation using graphene-plasmonic hybrid nanoarray, Nano Lett. 19 (2019) 8138–8148, https://doi.org/10.1021/acs.nanolett.9b03402.
[147] W. Weng, X. Sun, B. Liu, J. Shen, Enhanced fluorescence based on graphene self-assembled films and highly sensitive sensing for VB12, J. Mater. Chem. C 6 (2018) 4400–4408, https://doi.org/10.1039/C7TC05789J.
[148] S. Pandit, S. Seth, A. Bapli, S. Bhattacharjee, D. Seth, Graphene oxide induced prototropism in different solvents: enhancement of fluorescence induced by graphene oxide, J. Mol. Liq. 369 (2023) 120880, https://doi.org/10.1016/j.molliq.2022.120880.
[149] R. Wang, H. Liu, T. Xu, Y. Zhang, C. Gu, T. Jiang, SERS-based recyclable immunoassay mediated by 1T-2H mixed-phase magnetic molybdenum disulfide

probe and 2D graphitic carbon nitride substrate, Biosens. Bioelectron. 227 (2023) 115160, https://doi.org/10.1016/j.bios.2023.115160.
[150] J. Chen, D. Zhou, Z. Chen, X. Liu, Y. Xu, L. Guo, Enhanced polymeric carbon nitride nanosheet-based fluorescence for biosensing applications, ACS Appl. Nano Mater. 6 (2023) 1441–1447, https://doi.org/10.1021/acsanm.2c05202.
[151] J. Hasan, S. Bok, Plasmonic fluorescence sensors in diagnosis of infectious diseases, Biosensors 14 (2024) 130, https://doi.org/10.3390/bios14030130.
[152] T. Špringer, M. Bocková, J. Slabý, F. Sohrabi, M. Čapková, J. Homola, Surface plasmon resonance biosensors and their medical applications, Biosens. Bioelectron. 278 (2025) 117308, https://doi.org/10.1016/j.bios.2025.117308.
[153] H. Cao, L. Guo, Z. Sun, T. Jiao, M. Wang, Surface-enhanced fluorescence and application study based on Ag-wheat leaves, Chin. Phys. B 31 (2022) 37803, https://doi.org/10.1088/1674-1056/ac1f0d.
[154] C.-T. Huang, F.-J. Jan, C.-C. Chang, A 3D plasmonic crossed-wire nanostructure for surface-enhanced Raman scattering and plasmon-enhanced fluorescence detection, Molecules 26 (2021) 281, https://doi.org/10.3390/molecules26020281.
[155] H. Li, Q. Chen, M.M. Hassan, Q. Ouyang, T. Jiao, Y. Xu, et al., Au NS@Ag core-shell nanocubes grafted with rhodamine for concurrent metal-enhanced fluorescence and surfaced enhanced Raman determination of mercury ions, Anal. Chim. Acta 1018 (2018) 94–103, https://doi.org/10.1016/j.aca.2018.01.050.
[156] A. Yuan, X. Wu, X. Li, C. Hao, C. Xu, H. Kuang, Au@gap@AuAg nanorod side-by-side assemblies for ultrasensitive SERS detection of mercury and its transformation, Small 15 (2019) 1901958, https://doi.org/10.1002/smll.201901958.
[157] G. Satpathy, G.K. Chandra, E. Manikandan, D.R. Mahapatra, S. Umapathy, Pathogenic Escherichia coli (E. coli) detection through tuned nanoparticles enhancement study, Biotechnol. Lett. 42 (2020) 853–863, https://doi.org/10.1007/s10529-020-02835-y.
[158] P. Sevilla, F. García-Blanco, J.V. García-Ramos, S. Sánchez-Cortés, Aggregation of antitumoral drug emodin on Ag nanoparticles: SEF, SERS and fluorescence lifetime experiments, Phys. Chem. Chem. Phys. 11 (2009) 8342–8348, https://doi.org/10.1039/B903935J.
[159] D. Zhao, J. Yang, R. Jin, X. Hou, C. Li, W. Chen, et al., Seed-mediated synthesis of polypeptide-engineered stabilized fluorescence-enhanced core/shell Ag_2S quantum dots and their application in pH sensing and bacterial imaging in extreme acidity, ACS Sustainable Chem. Eng. 7 (2019) 13098–13104, https://doi.org/10.1021/acssuschemeng.9b02294.
[160] D.-P. Li, P. Zhang, X. Guo, T. Zhang, X. Ran, T. Zhang, et al., A new fluorescent probe for detection of hydrazine and extremely acidic pH in different modes, Tetrahedron 159 (2024) 134007, https://doi.org/10.1016/j.tet.2024.134007.
[161] B. Liu, Y. Tan, Q. Hu, Y. Wang, Y. Mao, P. Tao, et al., A new ratiometric and colorimetric fluorescent Th^{4+} probe under extreme acidity and cell imaging, Sensor. Actuat. B-Chem. 296 (2019) 126675, https://doi.org/10.1016/j.snb.2019.126675.
[162] S. Wang, F. Li, L. Wang, R. Pan, L. Ma, Y. Yang, et al., Effective protection strategy of Surface-enhanced Raman scattering substrate in deep-sea cold seep in-situ detection, Chem. Eng. Sci. 308 (2025) 121422, https://doi.org/10.1016/j.ces.2025.121422.
[163] S. Wang, R. Pan, W. He, L. Li, Y. Yang, Z. Du, et al., In situ surface-enhanced Raman scattering detection of biomolecules in the deep ocean, Appl. Surf. Sci. 620 (2023) 156854, https://doi.org/10.1016/j.apsusc.2023.156854.
[164] S. Wang, F. Li, Z. Luan, L. Li, S. Xi, Z. Du, et al., Novel SERS probe based on Ag nanobean/Cu foam for deep-sea extreme environment biomolecule detection, ACS Sens. 9 (2024) 2402–2412, https://doi.org/10.1021/acssensors.4c00082.
[165] D. Hu, J. Xiang, J. Guo, C. Wang, J. Qi, B. Li, et al., Paper and cloth-based microfluidic chips for rapid cysteine detection in deep-sea cold seeps, Analyst (2025), https://doi.org/10.1039/D5AN00109A.
[166] R. Du, D. Yang, G. Jiang, Y. Song, X. Yin, An approach for in situ rapid detection of deep-sea aromatic amino acids using laser-induced fluorescence, Sensors 20 (2020) 1330, https://doi.org/10.3390/s20051330.
[167] E.J. Eshelman, M.J. Malaska, K.S. Manatt, I.J. Doloboff, G. Wanger, M.C. Willis, et al., WATSON: in situ organic detection in subsurface ice using deep-UV fluorescence spectroscopy, Astrobiology 19 (2019) 771–784, https://doi.org/10.1089/ast.2018.1925.
[168] S. Sunuwar, C.E. Manzanares, Low temperature fluorescence excitation and emission spectra of molecules relevant to Mars: Chlorobenzene, benzoic acid, phthalic acid, mellitic acid, and benzene in water ice solutions at temperatures between 78 K and 273 K, Planet, Space Sci. 257 (2025) 106054, https://doi.org/10.1016/j.pss.2025.106054.
[169] S. Tang, B. Chen, C.P. McKay, R. Navarro-Gonzálezv, A.X. Wang, Detection of trace organics in Martian soil analogs using fluorescence-free surface enhanced 1064-nm Raman Spectroscopy, Opt. Express 24 (2016) 22104–22109, https://doi.org/10.1364/OE.24.022104.
[170] M. Marečková, M. Barták, J. Hájek, Temperature effects on photosynthetic performance of Antarctic lichen Dermatocarpon polyphyllizum: a chlorophyll fluorescence study, Polar Biol. 42 (2019) 685–701, https://doi.org/10.1007/s00300-019-02464-w.